Vilnius University
Faculty of Physics

Dominykas Kandrotas

OPTIMIZATION OF INTRINSIC STRESS IN SiO_2 THIN FILMS DEPOSITED BY DUAL ION BEAM SPUTTERING AND ITS IMPACT ON MULTILAYER HIGH-REFLECTANCE COATINGS

Master's final thesis
Photonics and Nanotechnology study programme

Student	Dominykas Kandrotas
Academic supervisor	dr. Sabina Kuprėnaitė
Director of the Institute	prof. dr. Ramūnas Aleksiejūnas
Reviewer	dr. Tomas Grinys

Vilnius 2026

Table of Contents

1. Introduction

SiO_2 layers deposited by ion beam sputtering (IBS) exhibit significant compressive stress, often exceeding that of other materials commonly used in interference coatings, such as HfO_2, Ta_2O_5, Al_2O_3, and TiO_2. In multilayer optical coatings, high compressive stress can degrade substrate flatness and introduce optical aberrations that may distort the wavefront, change the beam shape, or reduce the overall optical performance of the system [1]. Several methods are commonly used to reduce these stress-related effects. One approach is the deposition of stress compensation coatings (SCC) on the opposite side of the substrate to restore flatness [2]. Another widely used method is ex-situ thermal annealing, which allows the deposited films to relax and reduce their residual stress. However, previous studies have shown that dual ion beam sputtering (DIBS) can also reduce intrinsic stress directly during deposition, resulting in lower stress values already in the as-deposited state [3].

Reducing intrinsic stress during deposition is especially important because additional stress compensation coatings or thermal annealing are not always possible in practical optical systems. In applications such as thin-disk laser coatings, diffraction gratings, crystalline optical substrates, or very thin optical components, backside coating deposition may be limited or impossible due to optical, thermal, or mechanical constraints [4]. Similarly, high temperature annealing may not be compatible with temperature-sensitive substrates or complex optical structures. Therefore, achieving lower residual stress directly during the deposition process remains highly important for advanced optical coating applications.

This work investigates the influence of assisting ion source parameters and ex-situ annealing on the residual stress and optical properties of SiO_2 thin films deposited by DIBS technology. Based on the obtained monolayer results, optimized deposition parameters were selected for the fabrication of multilayer high-reflectivity coatings, which were then compared with coatings deposited without the assisting ion source.

The main objective of this work was to investigate the influence of assisting ion source parameters and ex-situ annealing on the residual stress of SiO_2 films and multilayer optical coatings deposited by ion beam sputtering.

Main tasks of this work:

1. Deposit SiO_2 monolayers using dual ion beam sputtering while varying the assisting ion source parameters.

2. Investigate the influence of assisting ion source parameters and ex-situ annealing on the residual stress and optical properties of the deposited SiO_2 monolayers.
3. To deposit a 1064 nm high-reflectivity multilayer coating using optimized assisting ion source parameters.
4. Compare the stress relaxation and optical characteristics of multilayer coatings deposited with and without the assisting ion source before and after *ex-situ* annealing.

2. Literature review

2.1. Structure zone model.

The structure zone model is the pivotal pillar in the study of thin films, which provides the understanding of the morphological evolution of thin films as functions of the conditions in which deposition takes place. This model was originally introduced by Movchan and Demchishin in 1969 and it lets us correlate variables such as substrate temperature and working gas pressure with microstructural features of thin films [5]. It was later modified and improved by Thornton in 1974 by adding a second axis to the structure zone model diagram which incorporated the pressure of sputtering gas and the homologous temperature, which is the substrate temperature divided by the temperature of the thin film material [6]. The Thornton model can be seen in Figure 1.

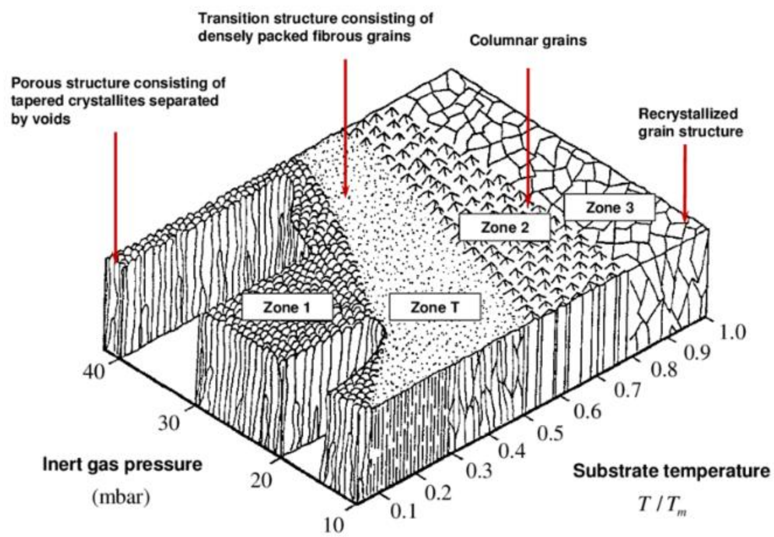

Figure 1. Thornton structure zone model [5].

This model is separated into four zones, which appear during deposition processes:

- **Zone 1**: Porous, column shaped structures with low density and sub-par adhesion, this type of structures are formed at high pressures and low substrate temperatures.
- **Zone T**: Also known as the transition zone with more tightly packed features, fibre-like grains which indicates improved surface diffusion and mobility of adatoms.
- **Zone 2**: Much denser columnar grains than in Zone 1. Has defined boundaries. Deposited under higher substrate temperatures.

- **Zone 3**: Achieved at very high (near melting temperature) substrate temperatures, no longer has columnar structure, but grains of various shapes which are isotropic, this is a result of high atomic mobility.

The structure zone model enables the tailoring and fine tuning of thin film properties depending on the application. Using the model, it is possible to engineer films with desirable optical, mechanical, thermal and electrical characteristics, for example Zone 2 structures are more sought after in applications requiring excellent mechanical strength and resistance to wear, while on the other hand, Zone 1 structures are more suitable for applications needing more porous or low thermal conductivity applications [7]. These days, plasma-based techniques are mostly used in thin films deposition, and for these types of deposition an expansion to the Thornton model was created by Andre Anders (Figure 2), in which the homologous temperature is replaced by generalized temperature T* and the linear pressure axis is replaced by a logarithmic axis of energy flux E* and a z-axis for film thickness [8].

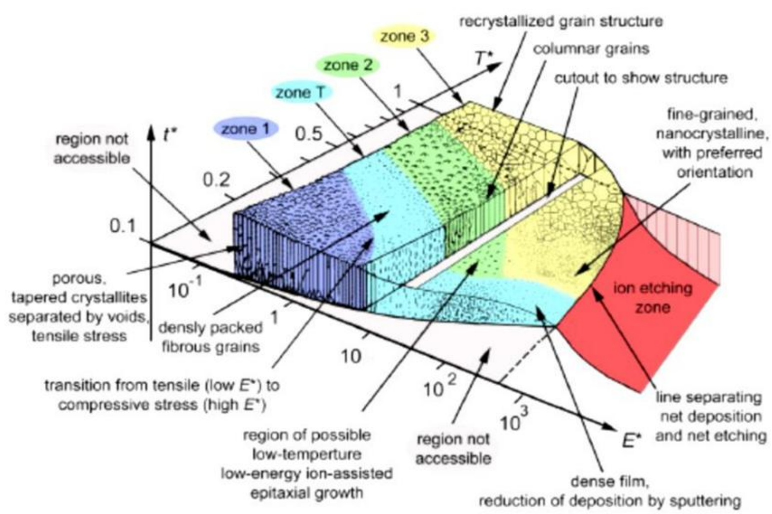

Figure 2. Anders's structure zone model [8].

All these changes to the Thornton model are made to acknowledge heating and displacement effects caused by ion bombardment in plasma-based deposition techniques. The evolution of the structure zone model depicts the growth in sophistication of thin film technologies and the need for special materials with custom nanostructures. This in turn shows that the structure zone model remains an especially important part of thin film technologies, to predict and understand film microstructure.

2.2. Mechanical stress in thin films.

Mechanical stress induced by deposition in thin film technologies play a crucial part in the longevity, mechanical stability of the film. In addition, the deposited thin film can deform and bend the substrate and in turn distort the wavefront reflecting or passing through a component. There are two types of mechanical stress which are induced in thin film technologies – tensile or compressive.

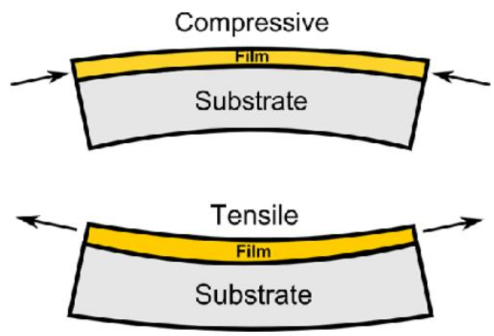

Figure 3. Difference between compressive and tensile stress [9].

It is possible to determine the mechanical stress in deposited thin films experimentally by using the Stoney formula, shown in Eq. 1 [10]:

$$\sigma = \frac{1}{6}\left(\frac{1}{R2} - \frac{1}{R1}\right)\frac{E_s}{(1 - v_s)}\frac{t_s^2}{t_f} \tag{1}$$

where E_s is Young's modulus of the substrate, t_s is the substrate thickness, t_f is the coating thickness, v_s is Poisson's ratio for the substrate R2 is the radius of curvature of the substrate after deposition and R1 is the radius of curvature before deposition. Thin films deposited using sputtering technologies (ion beam or magnetron sputtering)exhibit high compressive stress, in the range of ~200 MPa. Studies have found that ion beam sputtered SiO_2, had a stress value of five times larger than Ta_2O_5 [1]. High compressive stress in ion beam sputtered films emerge from the atomic peening effect. In ion beam sputtering, high energy ions (usually Ar^+) are employed to sputter target material. During this process, these ions might reflect and strike the growing film. These impacts can penetrate the thin film surface and in turn displace some atoms beneath. Penetration of the thin film further pushes the atoms together and compressive stress builds up overtime, on the other hand, this effect leads to very dense and smooth film [12]. Both these materials are often used in high-reflective coatings as low and high refractive index materials respectively. It is very important to control the stress of multi-layer coatings, to minimize wavefront distortions and deformations in optical coatings. This can be done by controlling deposition conditions, such as ion energy, gas pressures or implementing an assistant ion source, in addition to the primary ion source.

Mechanical stress in thin films is usually evaluated through the measurement of substrate flatness, because the stresses inside the coating deform the optical surface. After the deposition of a thin film on a substrate, the intrinsic stresses inside the coating create a bending force which changes and distorts the shape of the optic. The strength or amount of deformation is commonly described using flatness values of $\lambda/2$, $\lambda/5$, $\lambda/10$. These values represent the deviation of the measured surface from the ideally flat surface relative to the wavelength of the light source used in the measurement. In most cases, a He-Ne laser with the wavelength of 632.8 is used as the light source. So, for example, a flatness value of $\lambda/10$ means that the maximum surface deviation (peak to valley) is approximately 63 nm. Optical flatness is typically measured using interferometric methods such as Fizeau or Michelson interferometry where interference fringes reveal the surface deformation of the coated substrate.

2.3. Intrinsic Stress Control in IBS Thin-Film Optics

2.3.1. Dual Ion Beam Sputtering (DIBS)

To reduce the intrinsic stress commonly observed in IBS coatings, several modified deposition approaches have been developed. One of these methods is dual ion beam sputtering (DIBS), which introduces additional control over the film growth process and coating properties.

DIBS technology is a sputtering technique commonly used in optical thin film deposition, where a secondary ion source is directed at the substrates on which the film is being sputtered. While the primary beam sputters a metal or metal oxide target, the assisting ion source controls the film growth at the substrate surface [12]. As discussed before, conventional IBS or other sputtering techniques often develop high compressive stress due to atomic peening caused by energetic particle bombardment. The DIBS approach provides improved control over film density, microstructure, stoichiometry, and residual stress. As a result, DIBS coatings generally exhibit lower compressive stress while preserving the high optical quality and low surface roughness characteristic of IBS films [3].

Compressive stresses as low as 48 Mpa were reached using the help of an assist ion source and different accelerating voltages in assist ion source (Figure 4) [13]. This is a tenfold decrease in compressive mechanical stress, compared to SiO_2 deposited with standard ion beam sputtering [14].

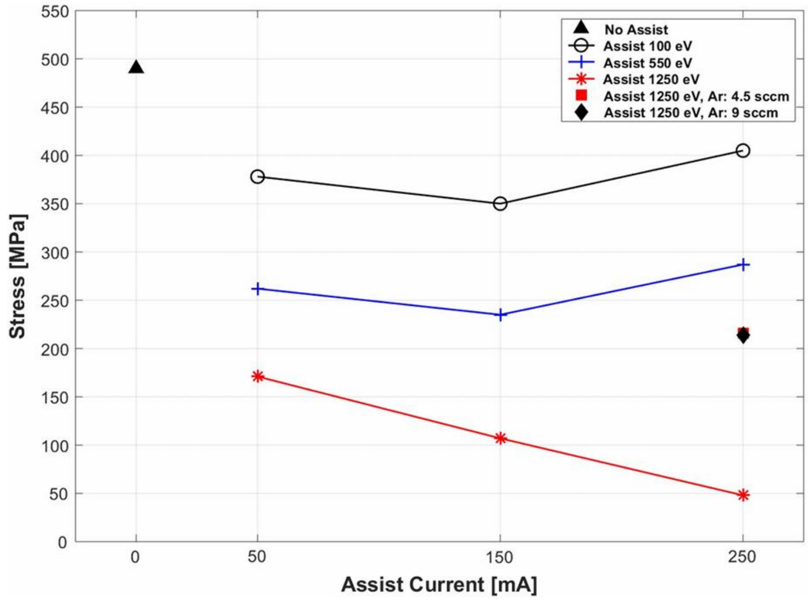

Figure 4. Stress vs. assist ion source energies [13].

Figure 5 shows another way of controlling the stress changing ion beam current of the auxiliary ion source [15].

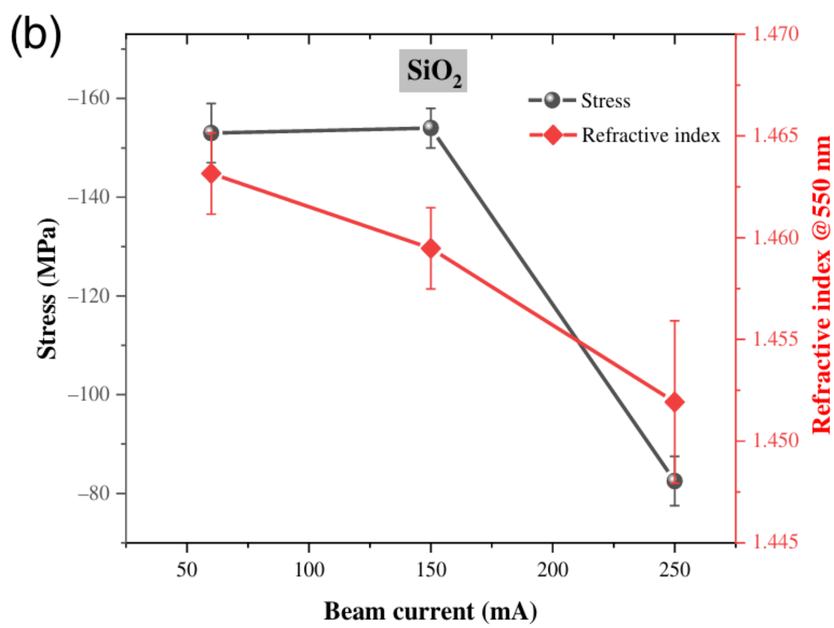

Figure 5. Effects of different auxiliary ion beam currents on the optical and mechanical properties of SiO_2 thin film. [15]

A high-energy assist ion beam can lead to a reduction in internal stress of the film, as it weakens the energy of the primary ion beam. This diminished energy results in less effective bombardment of the IBS film, disrupting the formation of its originally dense structure, this can be also applied to systems without a secondary ion beam, but with smaller effects [16].

2.3.2 *Ex-situ* and *In-situ* annealing

Ex-situ annealing is one of the most widely used techniques to diminish internal stresses created by sputtering dense films and to improve coating stability after deposition. During this annealing process, a coated substrate is heated in a controlled environment for a defined period. Such thermal treatment allows structural relaxation and reduces growth-related defects [17]. Annealing increases atomic mobility and enables local rearrangement of the amorphous network which reduces the mechanical stress stored within the coating. Studies have shown that for materials used in this work, such as IBS deposited Tantalum Pentoxide (Ta_2O_5) reaches around -200 Mpa [17], while Silicon Dioxide (SiO_2) can reach up to -700 Mpa compressive stresses [18]. The effects of ex-situ annealing of Ta_2O_5 can be seen in Figure 6. A clear dependency can be seen between the residual stress and annealing temperature, where the stress becomes decreasingly compressive (negative MPa value) with the increase of temperature and even becomes tensile at extremely high temperatures.

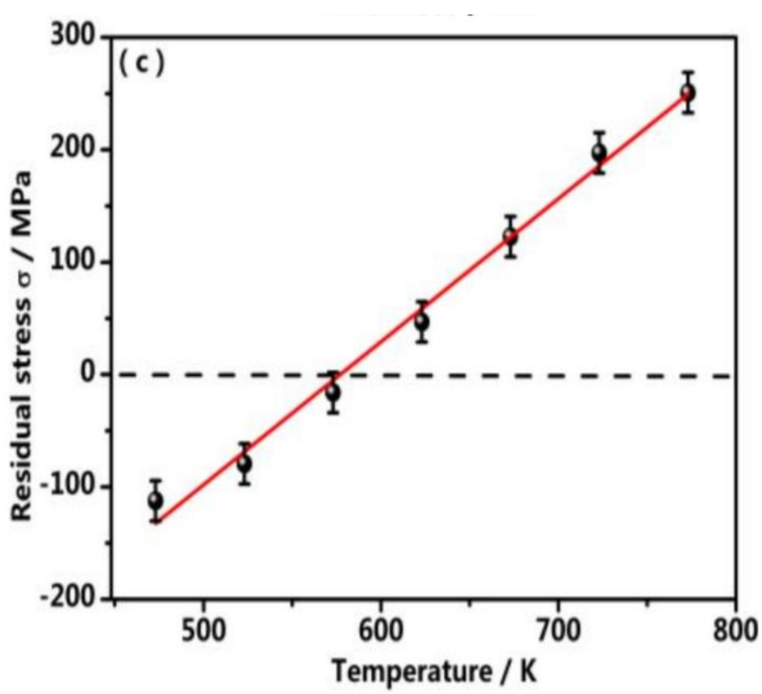

Figure 6. The stress of the Ta2O5 films with thicknesses of 500 nm annealed at different temperatures; annealing temperatures are set at 473 K, 523 K, 573 K, 623 K, 673 K, 723 K, and 773 K, respectively [17]

SiO_2 also shows this dependency and it can be seen in Figure 7.

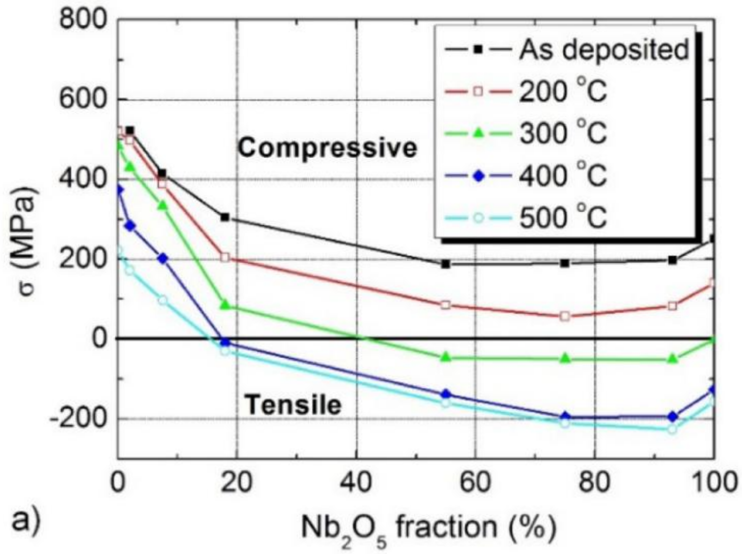

Figure 7. Residual stress according to Nb2O5 fraction in monolayer mixture at different annealing temperatures. AFM measurements of pure Nb2O5 before and after annealing to 500 °C [18]

In this study the researchers deposited various Nb_2O_5–SiO_2 mixtures by sputtering. The sample containing 0% Nb_2O_5 can be treated as a pure SiO_2 single layer. The as-deposited films exhibited compressive stress values of approximately 500 MPa. With increasing annealing temperature, the magnitude of the compressive stress gradually decreased. After annealing at 500 °C the stress was reduced to roughly 200 MPa [18].

In-situ thermal annealing during the coating process could be another approach for reducing stress in growing optical thin films. IBS coatings are typically very dense and non-porous which results in high compressive stress caused by energetic particle bombardment and atomic peening. During standard IBS deposition the substrate temperature usually remains relatively low and commonly reaches only around 100–150 °C depending on the coating duration. If additional substrate heating is applied during deposition the atoms at the film surface gain higher mobility and can rearrange more easily as the coating grows. This allows partial structural relaxation to occur during deposition and reduces the buildup of intrinsic compressive stress inside the film [3].

2.3.3. Stress Compensating Coating (SCC)

Backside stress compensation coatings are commonly used to reduce substrate deformation caused by residual stress in optical thin films. This effect becomes especially significant for thin substrates and high layer count optical stacks. To compensate for this deformation an additional coating is deposited on the backside of the substrate. The backside coating generates an opposing bending moment which balances the stress produced by the front side coating and reduces the overall substrate curvature. In many cases the compensating layer does not need to have the same optical function as the front coating. Instead, the thickness and stress-thickness product are adjusted to achieve near-zero deformation of the optical component [19].

In some applications the backside coating must also satisfy optical requirements in addition to compensating stress. This is especially important in ultrafast laser systems where unwanted backside reflections can affect beam quality and measurement accuracy. A good example was demonstrated by Amotchkina et al. 2014 where the authors deposited a highly complex antireflection coating on the backside of a dispersive mirror substrate. The purpose of the coating was not only to suppress backside reflections but also to compensate the mechanical stress generated by the front side multilayer mirror coating. To achieve this the backside anti-reflective coating was designed with a similar total thickness and material distribution as the front side coating. The final anti-reflective coating design consisted of 71 layers with a total thickness of approximately 7.5 μm [20].

The group evaluated the effectiveness of the stress compensation using a Fizeau interferometer at a wavelength of 632.8 nm. They observed that substrates coated only on one side experienced a significant degradation in surface flatness from λ/10 to λ/4 due to coating stress. After deposition of the backside anti-reflective coating the original surface flatness was restored to approximately λ/10 which matched the uncoated substrate. These results confirmed that a properly designed backside optical coating can simultaneously provide optical functionality and nearly complete stress compensation.

2.4. Interference optical coatings.

Also known as thin-film coatings, use the effect of interference to selectively transmit, reflect or absorb light at specific wavelength. Interference coatings are mainly used for anti-reflective coatings, mirrors, filters, beams splitters [21]. When a light wave encounters a thin film with a different refractive index than its surrounding medium, part of the light is reflected, and part is transmitted at each interface. The multiple reflections within the layers produce interference effects. The resultant intensity of the reflected or transmitted light depends on the optical path difference (OPD) (Eq. 2) between the waves.

$$OPD = 2n_1 d cos(\theta) \quad (2)$$

where d is the physical thickness of the coating, n_1 refractive index of the coating, θ and of propagation within the film. Depending on the phase difference, interference can become constructive (amplification of reflected or transmitted wavefront) or destructive (suppression of reflected or transmitted wavefront). Conditions for constructive and destructive interference can be seen in Eq. 3 and Eq. 4 respectively:

$$2nd = m\lambda \tag{3}$$

$$2nd = (m + \frac{1}{2})\lambda \tag{4}$$

where n is the refractive index of the layer or coating, d physical thickness of the coating, λ wavelength of incident light and m=0,1, 2…, is the order of interference. Depictions of these conditions can be seen in Figure 8.

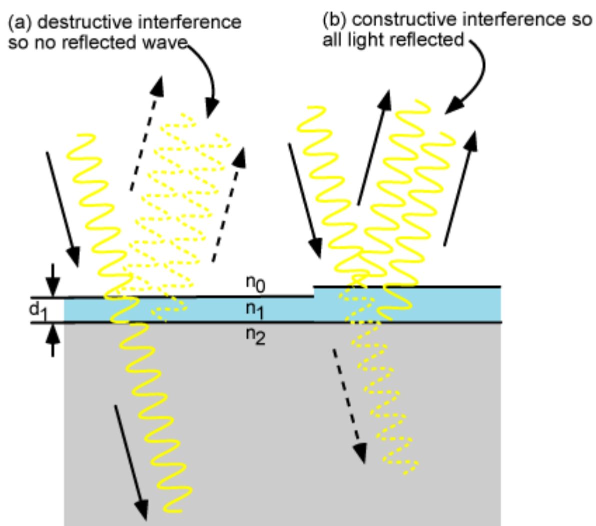

Figure 8. Destructive and constructive interference in thin films [22]

By combining alternating pairs of low and high refractive index materials, it is possible to manufacture not only anti-reflective coatings, but polarizers, filters, dichroic mirrors or high-reflective (HR) coatings. SiO_2 is often used as a low refractive index material in optical coatings, and that is why control of internal stress is important in this material.

3. Methodology

3.1. Substrate preparation

In this work thin films were deposited onto fused silica substrates with a diameter of 25.4 mm and thicknesses of 1 mm and 5 mm. 1 mm thickness substrates were used for flatness measurements, while the 5 mm thickness samples were used for spectrum measurements. Prior to deposition the substrates were cleaned using a fully automated four-stage ultrasonic cleaning system, Elma Evo, manufactured by Elma. The cleaning process began in a 40 kHz ultrasonic bath containing a pH 13 cleaning solution. Residual contaminants were then removed using tap water in the following stage of the cleaning system. After rinsing the substrates were washed in deionized water and subsequently dried. The dried substrates were visually inspected under a concentrated light source to ensure that no surface defects, dust particles, or other contaminants remained on the surface. After inspection the substrates were mounted into dedicated holders and installed into the coating deposition system.

Figure 9. Elma Evo industrial ultrasonic bath [23]

3.2. Spectrophotometer

Spectrophotometry is a method used to measure the transmission, reflection, and absorption properties of materials as a function of light wavelength. It primarily operates in the near-ultraviolet (UV), visible, and near-infrared (IR) regions of the electromagnetic spectrum. Spectrophotometers have wide-ranging applications across science and technology, including semiconductor and laser technologies, optics and photonics, printing and forensic analysis, as well as laboratory studies of materials, chemicals, and biological samples. The principal scheme of a spectrophotometer can be seen in Figure 7.

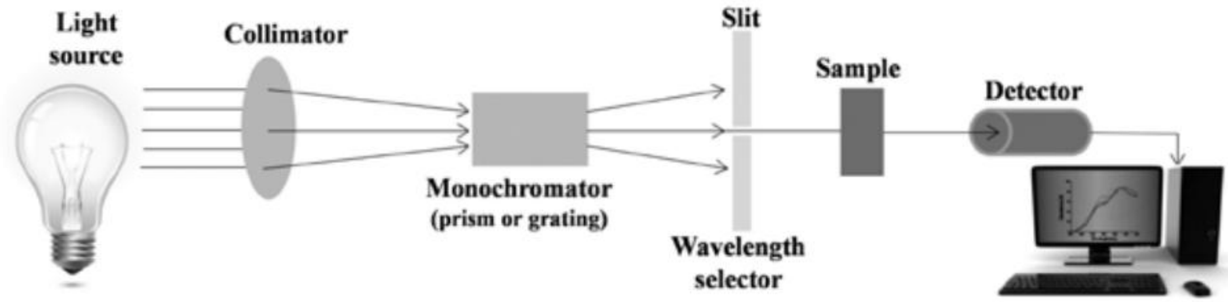

Figure 7. Principle scheme of a spectrophotometer [24].

Light emitted from the source lamp is first collimated and directed into a monochromator, where it is dispersed into its constituent wavelengths through diffraction. A narrow range of wavelengths is then selected using a mechanical slit positioned at the monochromator output. The selected light passes through the sample, and the transmitted intensity is detected and converted into absorbance or transmittance values.

The spectra of the SiO_2 monolayers deposited in this work were measured using Photon RT spectrophotometer made by Essent Optics [25]. An incidence angle of 8° was used because it was the minimum angle accessible for reflection measurements. Transmission measurements were conducted at the same angle, as measurements at normal incidence (0°) may cause undesirable back-reflections into the light source. The measured range was 185-950 nm for single layer coatings. Measurements of the Ta_2O_5/SiO_2 multilayer coatings were performed over the wavelength range of 864–1264 nm. Ultraviolet range measurements are possible because the spectrophotometer employs a deuterium lamp for ultraviolet measurements. For visible range measurements a simple halogen lamp is used. The resolution of the spectrophotometer is 0.3 nm in ultraviolet range and 0.6 nm in the visible range. Also, measurements were made in 1 nm step, with the averaging count of 20. The spectrophotometer used in this work contains four diffraction gratings, while light detection is performed using two detectors: a silicon (Si) detector for the 185–990 nm spectral range and a lead selenide (PbSe) detector for the 990–4900 nm spectral range. Other parameters such as slit size and the number of averaged spectra were adjusted for different spectral ranges to achieve the best possible signal-to-noise ratio.

3.3.Interferometer

An optical interferometer is a precision instrument used to evaluate the surface quality and planarity of optical flats, mechanical components, or wafers. The technique is non-contact and highly sensitive, capable of detecting deviations in surface flatness at the nanometre or even sub-nanometre level. The interferometer used in this work was the OptoFlat interferometer manufactured by Inter Optics. This appliance uses a coherent LED light source (633 nm wavelength) of small coherence length, which enables interference patterns to appear only from the first side of a clear substrate and not reach the backside. The principal scheme of such device can be seen in Figure 8.

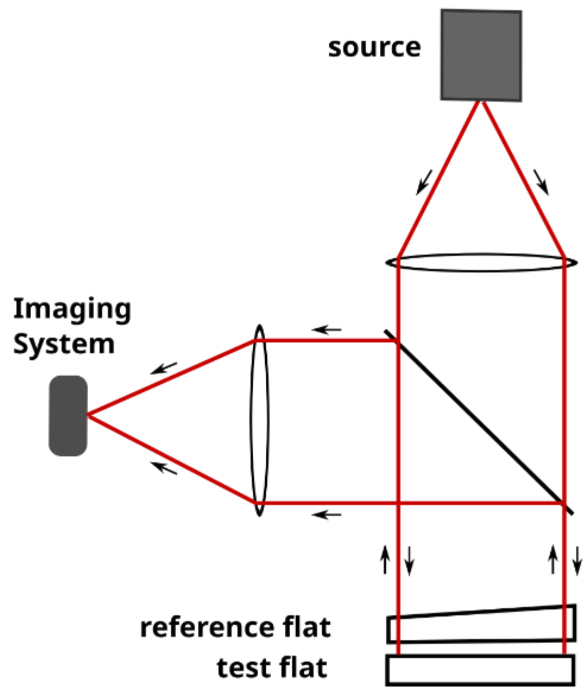

Figure 8. Principle scheme of a Fizeau interferometer [26].

The light created by the LED light source is split by a beamsplitter, one beam reflects from a mirror and the other one from the sample. The two reflected beams meet and form an interference pattern, depending on the type of interference (constructive or destructive). We can then in turn see minimums and maximums, which let us describe the flatness of the substrate. In this work, the flatness of the samples was measured at three stages: first for the uncoated substrates, then after thin-film deposition, and finally after the annealing process to evaluate coating-induced deformation and thermal stress effects. The stresses were calculated by using Eq. 1. Compressive stress is denoted in negative values, and tensile stresses are denoted by positive values. An example of flatness measurement report can be seen in Figure 9.

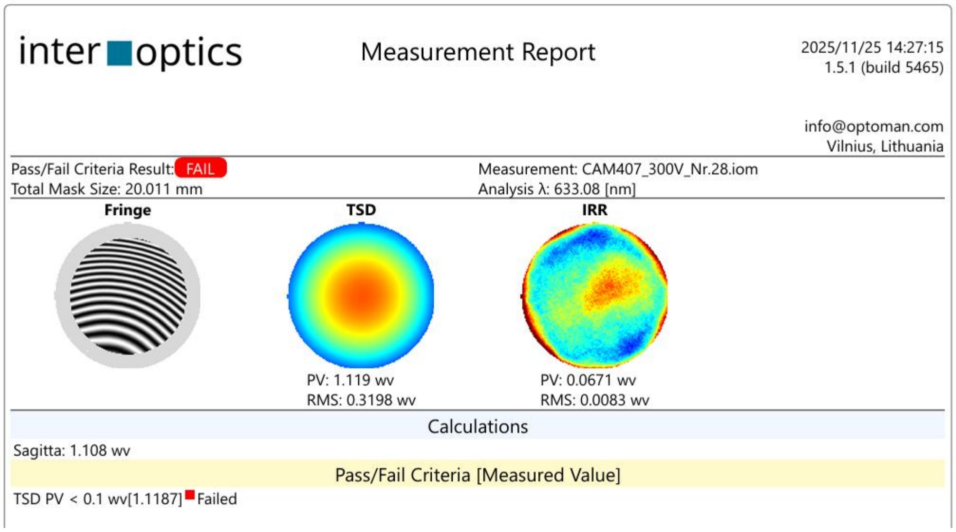

Figure 9. Flatness measurement report

Using formula (1), we can plug in the values to calculate stress for this measurement:

$$\sigma = \frac{1}{6}\left(\frac{1}{R2} - \frac{1}{R1}\right)\frac{E_s}{(1 - v_s)}\frac{t_s^2}{t_f} = \frac{1}{6}\left(\frac{1}{-7.01 * 10^{-7}} - \frac{1}{9.86 * 10^{-8}}\right)\frac{-7.17 * 10^{10}}{(1 - 0.17)}\frac{(10^{-3})^2}{5 * 10^{-7}} = -461\ MPa \qquad (5)$$

In formula (5) R2 and R1 values are Sagitta values multiplied by wavelength in meters, Young's modulus (E_s) for fused silica is $7.17 * 10^{10}$ Pa, Poisson's ratio (v_s) for fused silica is 0.17 and t_s (substrate thickness) and t_f (coating thickness) values are also in meters. Substrate without coating had the Sagitta measured to be 0.145 waves. The sign of Sagitta plugged into the formula is taken from the measurement. If the measurement shows compressive stress (TSD red in the centre) then the value of Sagitta is taken as negative, if the measurement shoes tensile stress (TSD blue in the centre), the value of Sagitta is taken as positive.

The figure shows a surface flatness measurement performed with the OptoFlat interferometer at a wavelength of 633 nm. The measurement consists of three main parts: the interference fringe pattern, the transmitted surface deformation (TSD) map, and the irregularity (IRR) map.

Fringe image shows the raw interference fringes formed by the reflected wavefront from the measured surface. The curvature of the fringes indicates that the sample surface is not perfectly flat and contains noticeable bending or curvature. TSD map represents the overall surface shape or low spatial frequency deformation of the optic. The reported PV (Peak-to-Valley) value of 1.119 waves means that the maximum height difference across the measured surface corresponds to approximately 1.119 wavelengths of the 633 nm laser light. IRR map shows the higher spatial frequency surface irregularities after removing the overall curvature and tilt. In this case the surface irregularity is relatively small with a PV value of 0.0671 waves and an RMS value of 0.0083 waves. This indicates that the local surface quality remains good despite the large overall bending.

The reported Sagitta value of 1.108 waves describes the total bow or curvature of the substrate surface relative to a reference flat surface. Such deformation is commonly observed in stressed optical coatings where residual stress causes bending of the substrate. The difference between PV (Peak-to-Valley) and Sagitta values can be seen in Figure 10.

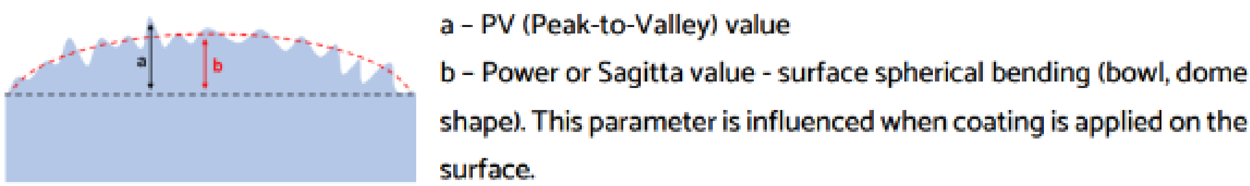

Figure 10. Schematic illustration of the peak-to-valley (PV) value and sagitta (power) used to characterize substrate surface deformation and coating-induced bending.

3.4.Annealing

For the *ex-situ* annealing of samples after deposition an electrical furnace (SNOL13-1100) with programmable annealing regimes was used. Samples were annealed at temperatures ranging from 350°C to 550°C with a step of 100°C. The annealing procedure was separated into three steps:

- Heating.
    - This step is done to gradually bring up the substrate up to the desired temperature.
- Retaining of temperature
    - To make sure that the sample reaches the needed temperature.
- Cooling
    - The sample and the furnace gradually cool down.

For the heating and cooling procedures, it was programmed to be 100° per one hour, and the temperature was retained for one hour after reaching the desired temperature.

3.5.Dual Ion-Beam sputtering system

Dual Ion-beam sputtering is a physical vapor deposition method where high-energy ions (usually Ar^+) accelerate to a metal, semiconductor or dielectric target using a three-grid system. These accelerated ions induce (1-2 keV) sputtering from the target and then in turn, atoms sputtered from the target deposit on substrates. These substrates are usually held in a circular holder which is spinning to produce a uniform thin film. The principal scheme of a Dual Ion-Beam sputtering can be seen in Figure 11.

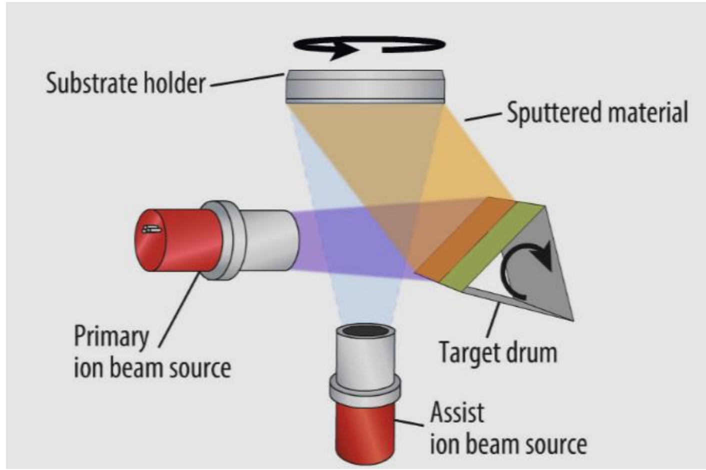

Figure 11. Principle scheme of a Dual Ion-Beam Sputtering machine [27].

In this work a NAVIGATOR 1000 IBS system, equipped with an assist ion source manufactured by Cutting Edge Coatings GmbH, was used for thin film deposition. Like all deposition technologies, ion-beam sputtering requires ultra-high vacuum base pressure (10^{-6} to 10^{-7} mbar), working pressure during deposition settles at around 10^{-3} to 10^{-4}. High pressure values ensure a clean and contaminant-free environment. These ultra-high vacuum values are reached using a system of a fore pump to reach pressures around 10^{-2} mbar and then a deep vacuum pump, such as a cryopump, to reach base pressure from deposition.

The ion plasma is created in a specially manufactured discharge chamber which is filled with inert gas. This argon gas is ionized using a radio frequency alternating electromagnetic field. For sputtering inert gas species are important, since different inert gases have different atomic mass, which has a significant impact for the sputtering process. For ion-beam sputtering argon is the most prominent inert gas used, while xenon is also used, it is usually too expensive. To extract this plasma, special ion-optics are used. Ion optics typically consist of three separate grids (Figure 12), each performing a distinct function: establishing the required initial plasma potential, accelerating the ions, and collimating them. This is achieved by applying different voltages to each grid.

As a result, a collimated and accelerated ion beam of a specific diameter emerges from the ion source through the grid system.

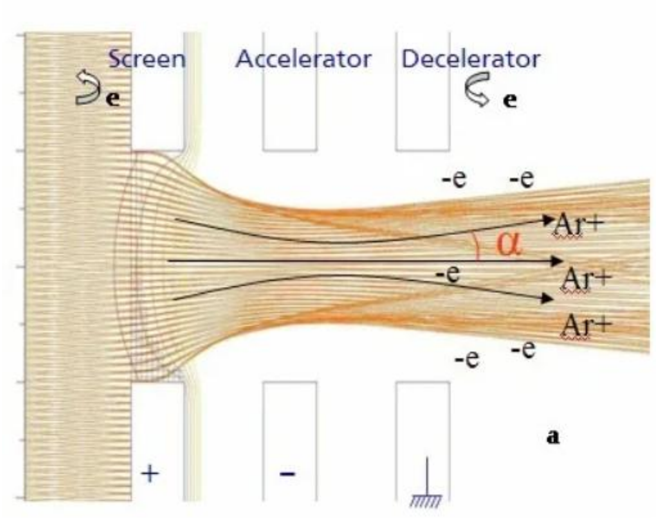

Figure 12. Ion beam sputtering grid system [28].

In addition to the grid, a neutralizer is used inside the coating chamber, which acts as an electron source. This source neutralizes the plasma and limits charge accumulation on substrates, target or other surfaces. When plasma is extracted through the grid system illustrated in Figure 10, ions are accelerated and subsequently neutralized before impinging on the target surface with sufficient kinetic energy to initiate atomic-scale sputtering of the target material. Sputter yield can be described as the number of target atoms ejected per incident ion [29]; this relation can be seen in Eq. 6:

$$\gamma = \frac{3}{4\pi^2}\alpha\frac{4M_1M_2}{(M_1+M_2)^2}\frac{E}{U_s} \tag{5}$$

Here, γ denotes the sputtering yield, defined as the ratio between the number of atoms ejected from the target and the number of incident ions. α is a dimensionless parameter that depends on the mass ratio and the ion energy. M_1 represents the mass of the incident ions, while M_2 denotes the mass of the target atoms. E is the energy of the ions striking the target, and U_s is the surface binding energy of the atoms at the target surface. In ion beam sputtering, dielectric films are predominantly deposited, requiring the introduction of pressurized oxygen into the vacuum chamber. Oxygen is directed into the path of the sputtered target atoms to facilitate reactive deposition. Due to the high kinetic energy of the sputtered atoms, the resulting thin film is characterized by a dense, non-porous microstructure.

After the cleaning procedure the fused silica substrates were mounted into a circular aluminium sample holder with a diameter of 270 mm (seen in Figure 13) and placed inside the coating chamber. The samples were positioned from the centre towards the outer edge of the holder during the sputtering process. The holder also contained an additional witness sample together with an empty reference position required for broadband monitoring (BBM). The witness sample was used for real time transmission spectrum measurements during deposition while the empty position was used to collect the reference signal from the light source. The BBM system used a halogen lamp emitting a broad visible range spectrum and the monitoring was performed in the 480–950 nm wavelength interval. During deposition the transmission spectrum of the witness sample was continuously monitored in real time. By analysing the spectral changes throughout the coating process the DIBS system could calculate the physical thickness of the growing thin film and accurately control the deposition process.

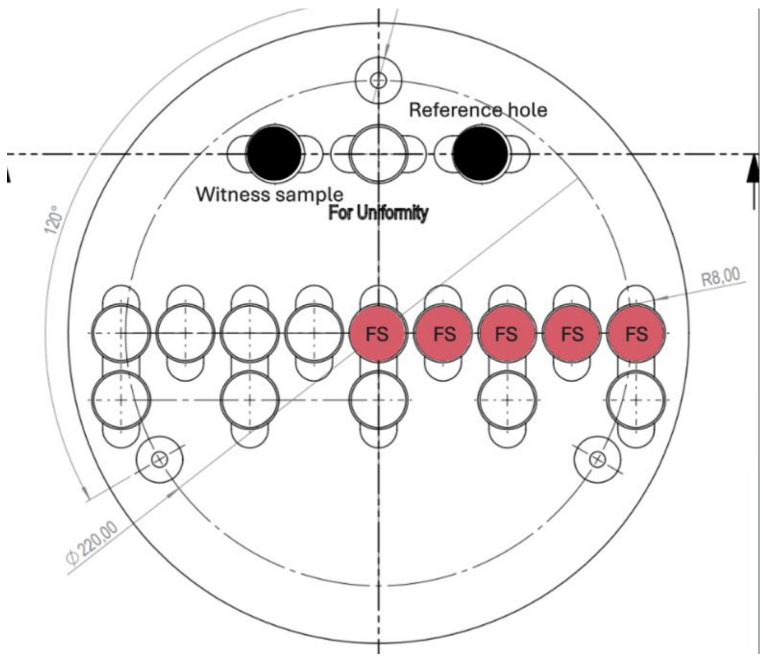

Figure 13. Sample holder used in this work

3.6.OptiLayer software

OptiLayer is a program dedicated to the design and characterization of thin films. The program allows users to create and characterize not only monolayer films but also complex multi-layer structures by carefully selecting coating materials, thicknesses of layers and the number of layers. OptiLayer software is separated into three different usages:

- Thin-film design, optical simulation and analysis (**OptiLayer**).
    - Allows users to design multilayer thin-film structures for specific optical properties
- Fitting experimental data (**OptiRE**).
    - Fits experimental data (e.g., spectrophotometer measurements) to theoretical models to determine actual layer parameters or deviations.

- Characterization of thin films (**OptiChar**)
    - Enables the characterization of refractive index, extinction coefficient, etc. from monolayer thin films when sputtered on substrates with known dispersions.

In this work, the initial design of the SiO_2 monolayer was modelled using OptiLayer software for sputtering using ion-beam sputtering. 500 nm thick monolayer was chosen for this work, because it creates enough minimums and maximums (Figure 12) for wavelength dependence of the refractive index calculations later in this work using a feature of OptiLayer called OptiChar.

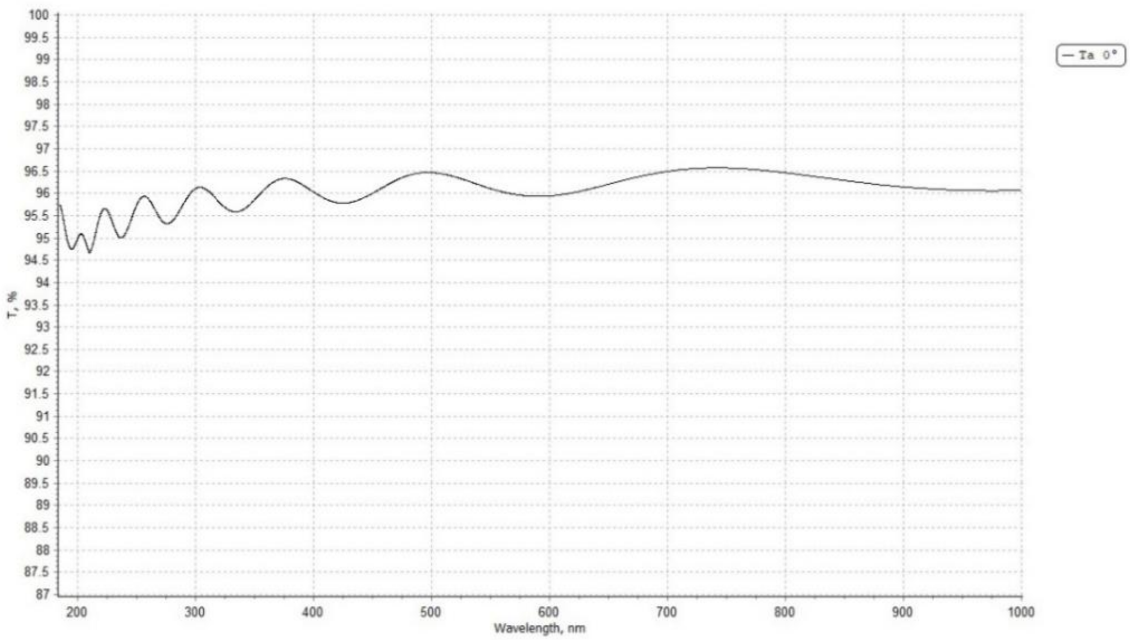

Figure 14. Theoretical unpolarized transmission spectrum of 500nm SiO2 thin film (UVFS substrate) at an incidence angle of 0°.

To calculate the wavelength dependence of the refractive index $n(\lambda)$, Cauchy model (Eq. 7) was used.

$$n(\lambda) = A + \frac{B}{\lambda^2} + \frac{C}{\lambda^4} + \cdots \quad (7)$$

where λ is the wavelength; A, B, C are empirical Cauchy coefficients determined by fitting experimental data. The measurements which were fitted to acquire the wavelength dependency of the refractive index, were transmission at an angle of 8° measured with the spectrophotometer mentioned in chapter 3.2.

For the multilayer design used in this work, a high-reflective coating with a modelled reflectance value of average polarization around 98% at 1064 nanometres and 0 degrees angle of incidence was sputtered using DIBS. The coating consisted of 13 layers of alternating Ta_2O_5 (~128 nm) and SiO_2 (~180 nm) materials. Such design was chosen because it includes materials that are widely used in optical coatings and at a wavelength that is a commonly used Nd:YAG laser operating wavelength. Nanosecond Nd:YAG lasers operating at 1064 nm are widely used in industrial material processing, laser micromachining, and laser damage threshold testing of optical coatings. Due to their high pulse energy and short pulse duration, these lasers are also commonly applied in LIDAR systems, nonlinear optics, medical procedures, and high-power laser research [30]. The theoretical multilayer high-reflective coating design used for sputtering can be seen in Figure 13.

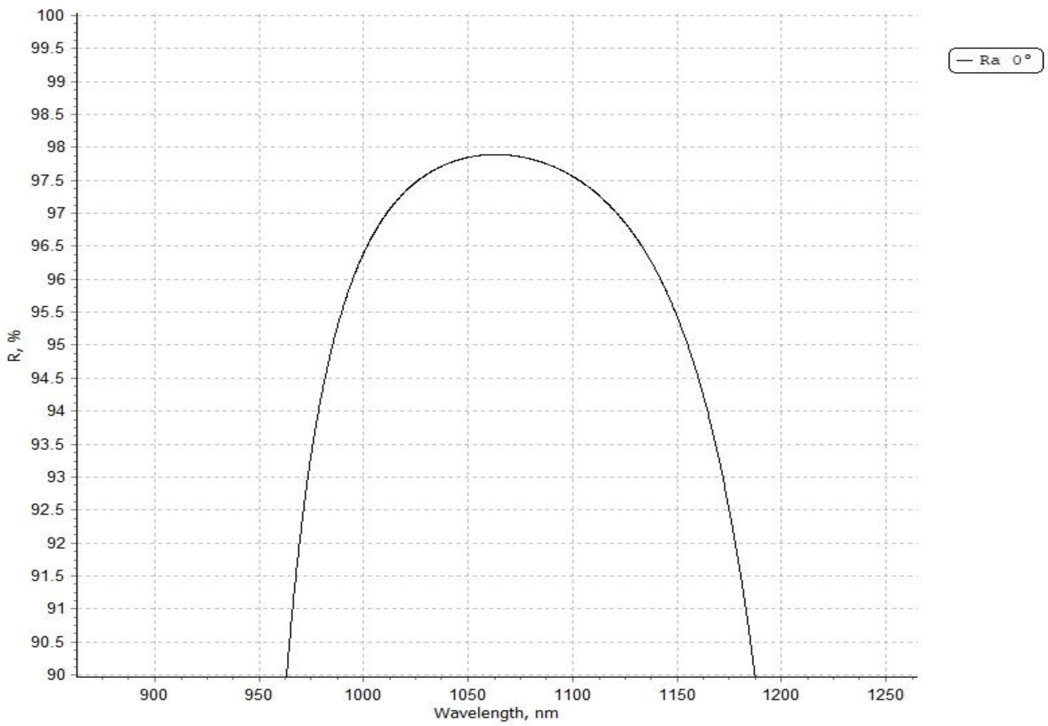

Figure 15. Theoretical design of the high-reflective coating sputtered in this work

4. Results and analysis

To investigate the influence of assisting ion source parameters on the residual stress of the deposited coatings, a series of SiO_2 single layer deposition experiments was performed. Throughout all experiments the primary ion source parameters were kept constant and the substrate holder position inside the deposition chamber remained unchanged. All deposited SiO_2 single layers had the same physical thickness of 500 nm. The parameters varied during the experiments were related only to the assisting ion source. These included the positive voltage corresponding to the ion accelerating voltage, the negative voltage corresponding to the ion beam collimating voltage, and the ionized gas flow rates of argon and oxygen. After evaluating the deposited single layers, the assisting ion source parameters that produced the best substrate flatness results were selected for multilayer coating deposition. An identical multilayer coating was also deposited without the assisting ion source to compare the resulting flatness values and evaluate the influence of the DIBS process on coating stress.

4.1. Influence of the accelerating ion voltage on the stress development in SiO_2 films

The first experiment was performed to investigate the influence of the assisting ion source accelerating voltage on the optical and mechanical properties of the deposited SiO_2 single layers. The positive voltage of the assisting ion source was varied from 250V to 450V with 350V chosen as the intermediate value. After deposition the transmission spectra of the samples were measured and used for optical characterization of the coatings. The dispersion relations, describing the wavelength dependence of the refractive index, were modelled using OptiChar software. The obtained optical models were then used to evaluate possible changes in film density and optical properties caused by different assisting ion source accelerating voltages. The experimental results of stress, transmission and wavelength dependency on the refractive index can be seen in Figure 16-17.

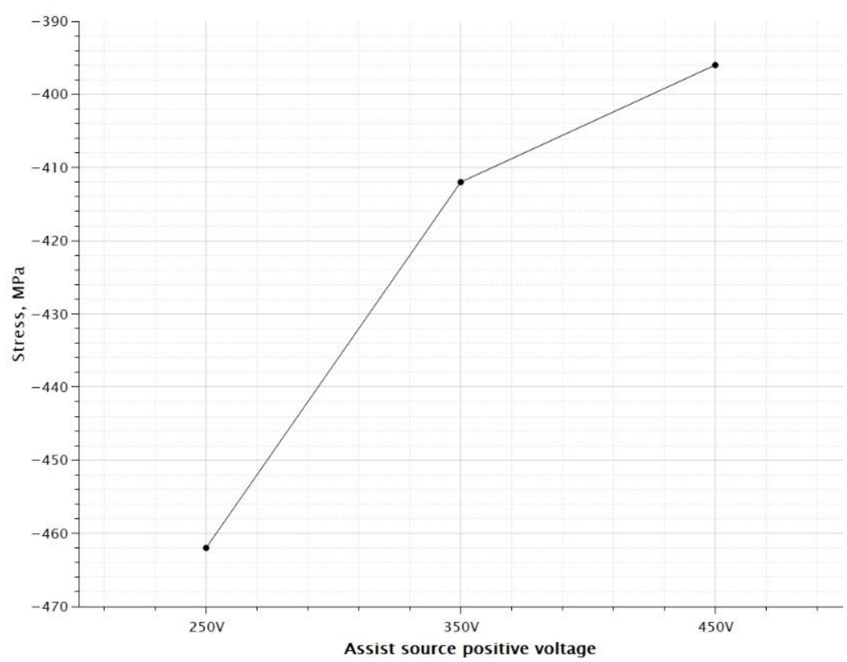

Figure 16. Stress dependency on accelerating ion voltage.

The results showed a clear dependence of residual stress on the assisting ion source accelerating voltage. The sample deposited with a 250 V accelerating voltage exhibited the highest compressive stress with values of approximately -460 MPa. Increasing the accelerating voltage gradually reduced the magnitude of the compressive stress, while the sample deposited at 450 V showed the lowest compressive stress of around -395 MPa. This behaviour is consistent with the observed deposition rates and changes in film growth conditions. The 250 V experiment produced the highest SiO_2 deposition rate of approximately 0.13 nm/s, while the deposition rate decreased to around 0.08 nm/s at 450 V. Lower deposition rates allow the adatoms on the growing film surface more time to rearrange and relax into energetically favourable positions, which can reduce the buildup of intrinsic compressive stress inside the coating.

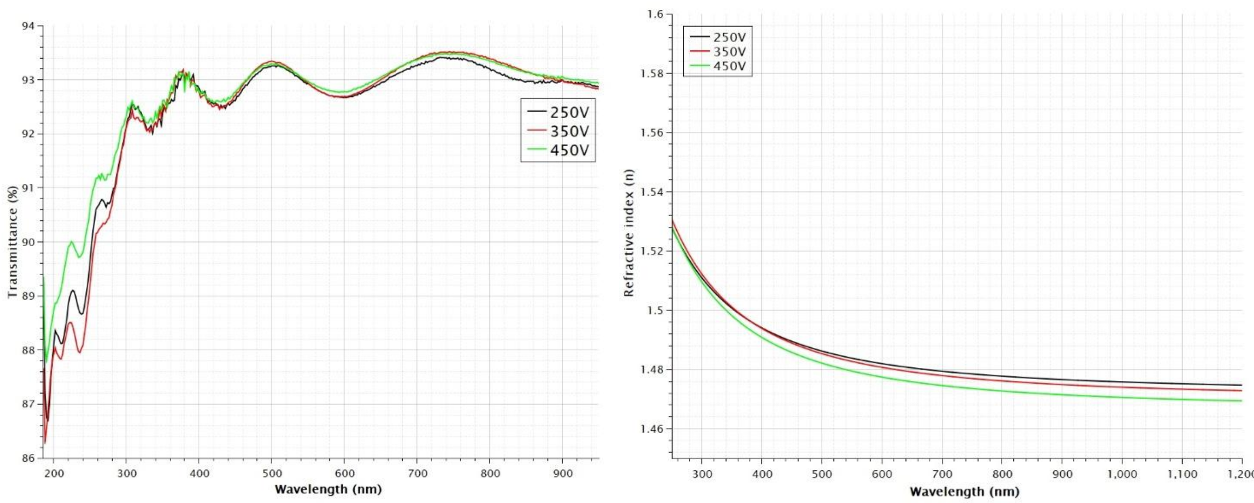

Figure 17. Measured spectral characteristics (left) and the corresponding refractive index dependence on wavelength (right).

The optical characterization results also showed a dependence on the assisting ion source accelerating voltage. Analysis of the transmission spectra revealed that the sample deposited at 450 V exhibited the lowest absorption near the UV absorption edge, indicating improved optical transparency compared to the other samples. The coatings deposited at 250V and 350V showed very similar spectral behaviour throughout the measured wavelength range.

The refractive index dispersion models obtained using OptiChar also followed a clear trend with accelerating voltage. The sample deposited at 250V exhibited the highest refractive index with a value of approximately $n = 1.478$ at 800 nm, while the 450V sample showed the lowest refractive index. This behavior may indicate that increasing the assisting ion source accelerating voltage leads to lower film density. Since denser IBS films are generally associated with stronger atomic peening and higher compressive stress, the reduced refractive index of the 450V coating is consistent with the lower stress values observed in the flatness measurements.

4.2. Effect of varying collimating ion source voltage in SiO_2 film stress

The second experiment investigated the influence of the assisting ion source negative voltage on the stress of SiO_2 monolayers. In a three-grid ion extraction system this voltage mainly affects ion beam collimation and the directionality of ions reaching the growing film. Therefore, changes in this parameter can influence the local ion flux at the substrate surface and the way energy is delivered during film growth. The experimental results of stress, transmission and wavelength dependency on the refractive index can be seen in Figure 18-19.

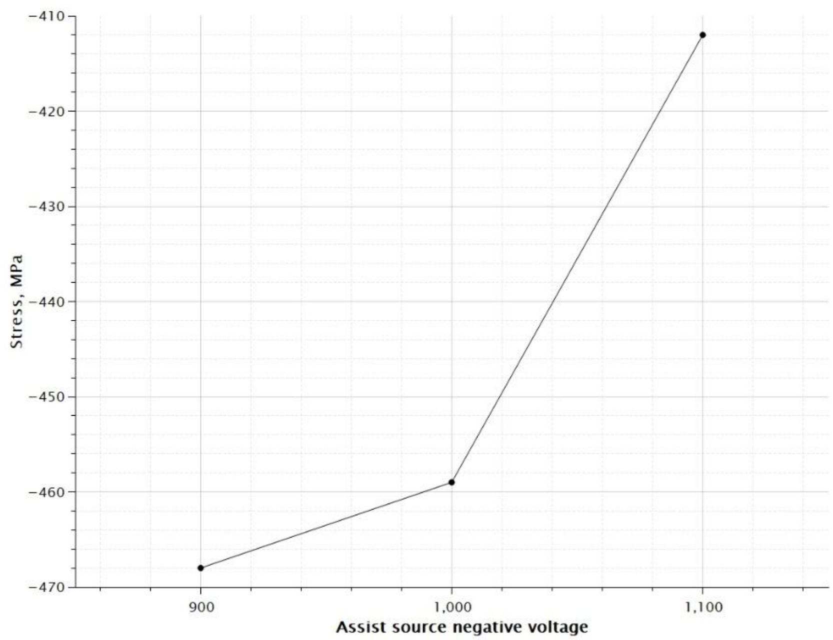

Figure 18. Stress dependency on collimating ion voltage.

Three negative voltage values were tested: 900V, 1000V, and 1100V. The coating deposited at 900V showed the highest compressive stress of approximately -470 MPa, while the 1100V experiment resulted in the lowest compressive stress. This trend also agrees with the measured deposition rates. At 900V the SiO_2 deposition rate was around 0.12 nm/s, whereas at 1100V it decreased to approximately 0.09 nm/s. The lower deposition rate at higher collimating voltage likely gave surface atoms more time to rearrange during growth, which reduced the buildup of compressive stress in the film.

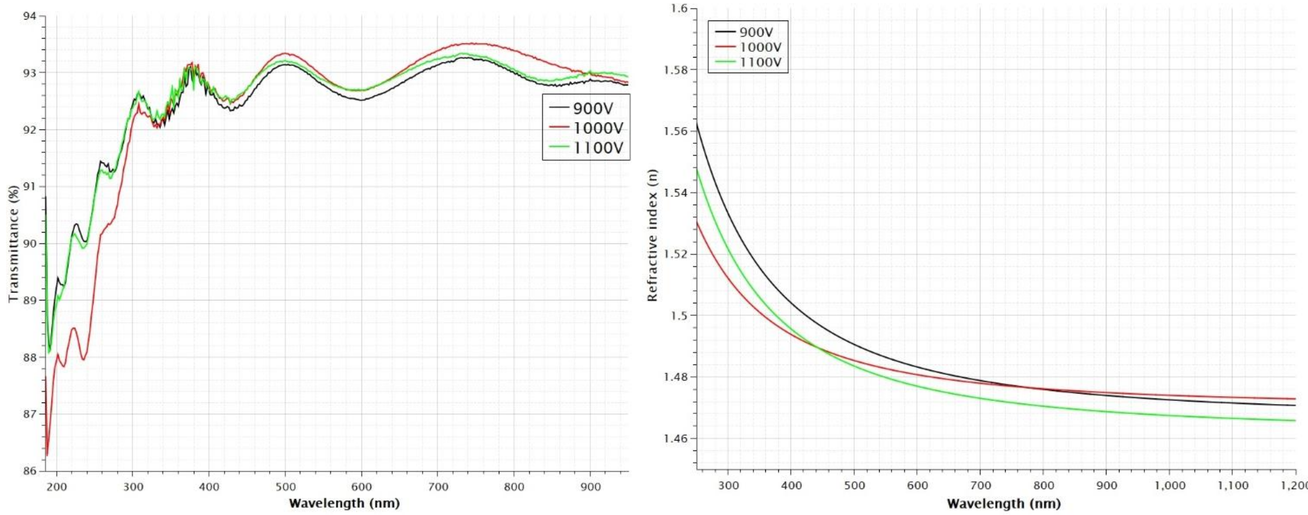

Figure 19. Measured spectral characteristics (left) and the corresponding refractive index dependence on wavelength (right).

The optical characterization results showed that the 900V and 1100V experiments had very similar transmission spectra both in the visible range and near the UV absorption edge, indicating that the optical losses of the coatings remained comparable. However, the refractive index dispersion models revealed noticeable differences between the samples. At 800 nm the coating deposited at 900V exhibited a refractive index of approximately $n = 1.475$, while the 1100V experiment showed a lower refractive index of around $n = 1.470$. This trend is consistent with the measured deposition rates and residual stress values. The coating deposited at 1100V had the lowest deposition rate and the lowest compressive stress, which suggests that the film was less densely packed. Since denser SiO_2 films generally exhibit higher refractive indices and larger compressive stresses due to stronger atomic peening, the lower refractive index of the 1100V coating agrees well with the observed reduction in stress.

4.3. Role of argon and oxygen flux from the assist ion source in SiO_2 films

The final experiment investigated the influence of the gas flux in the assisting ion source on the properties of the deposited SiO_2 single layers. In the assisting ion source, the supplied gases are ionized to form the plasma and the ion beam interacting with the growing film surface. Therefore, changes in the argon and oxygen gas flow rates can affect the energy transfer to the film, the etching conditions, and the overall growth dynamics during deposition. Throughout this experiment the assisting ion source accelerating and collimating voltages were kept constant, while only the reactive gas flux ratios were varied.

Three different reactive gas flow ratios with a total gas flow of 20 sccm were investigated: a 50/50 Ar/O_2 ratio consisting of 10 sccm Ar^+ and 10 sccm O_2 (named "10Ar10O2"), a 75/25 Ar^+/O_2 ratio consisting of 15 sccm Ar^+ and 5 sccm O_2 (named "15Ar5O2"), and a 25/75 Ar^+/O_2 ratio consisting of 5 sccm Ar^+ and 15 sccm O_2 (named "5Ar10O2"). The stress dependencies can be seen in Figure 20-21.

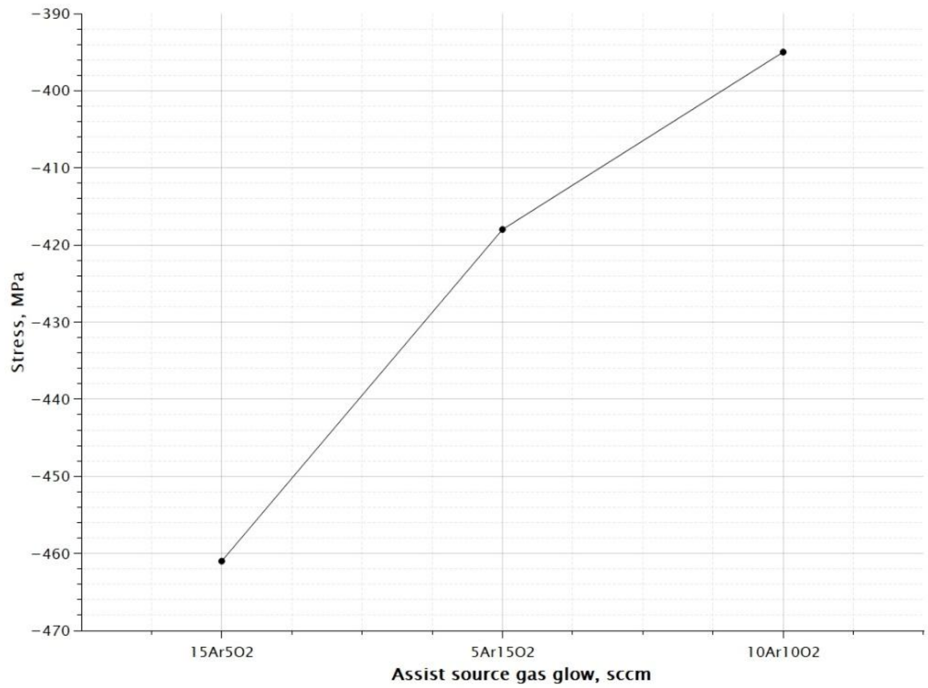

Figure 20. Stress dependency on argon and oxygen flux from the assist ion source

The residual stress values changed noticeably with different reactive gas flow ratios in the assisting ion source. The 75/25 Ar^+/O_2 ratio experiment resulted in the highest compressive stress of approximately −460 MPa, while the 25/75 Ar^+/O_2 ratio experiment reduced the stress to around -420 MPa. The lowest compressive stress of approximately -395 MPa was obtained using the balanced 50/50 Ar/O_2 ratio gas flow. The larger Ar^+ content likely increased the atomic peening effect due to the stronger physical bombardment of the growing film, leading to denser SiO_2 layers and higher compressive stress. Increasing the oxygen content reduced this effect and allowed the film structure to relax more during growth. The 50/50 Ar/O_2 ratio condition therefore provided the most favourable growth conditions for minimizing intrinsic stress in the deposited coatings. The spectral characteristics and refractive index dependency on the wavelength can be seen in Figure 19.

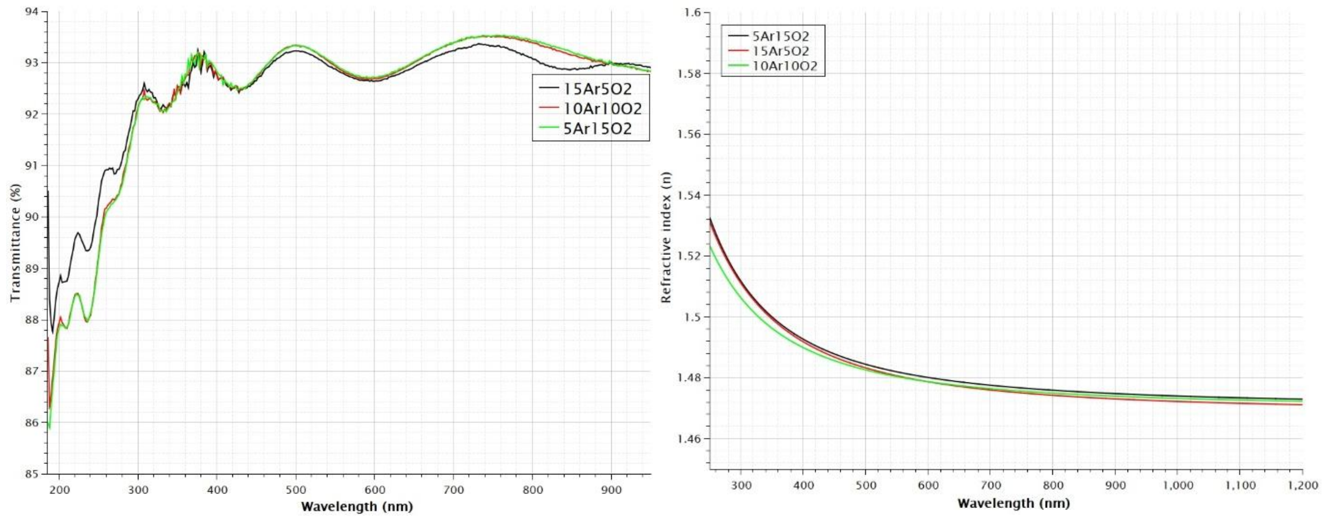

Figure 21. Measured spectral characteristics (left) and the corresponding refractive index dependence on wavelength (right).

The transmission measurements showed that the 75/25 Ar^+/O_2 ratio experiment exhibited the lowest absorption near the UV absorption edge, while the 50/50 Ar/O_2 and 25/75 Ar^+/O_2 ratio coatings had very similar spectral characteristics. The refractive index dispersion models also showed only small differences between all three experiments, which is consistent with the nearly identical SiO_2 deposition rates of approximately 0.11 nm/s. Since the refractive index values remained similar, the observed stress differences were likely influenced not only by film density but also by changes in the ion bombardment conditions during growth. The larger Ar^+ content in the 75/25 Ar^+/O_2 experiment likely increased momentum transfer to the growing film due to the heavier Ar^+ ions, which enhanced atomic peening and resulted in higher compressive stress. At the same time, the stronger bombardment may have reduced defect-related absorption in the UV range. In contrast, the balanced 50/50 Ar/O_2 condition likely provided more favourable growth conditions where the film could relax more efficiently during deposition, resulting in the lowest residual stress.

4.4. Stress relaxation behaviour under varying *ex-situ* annealing temperatures

To determine the stress relaxation under varying *ex-situ* temperatures, an electrical furnace was used (Chapter 3.3.). The temperatures at which the samples were annealed consisted of 350°C, 450°C, 550°C. Each experiment already mentioned was annealed to assess how different heating temperatures impact stress relaxation. To begin with, the samples from chapter 4.1. were annealed (Figure 22).

The annealing experiments showed that increasing the annealing temperature reduced the compressive stress for all deposited SiO_2 coatings, where the accelerating voltage was varied. The largest stress reduction was observed after annealing at 550°C, where the stress values decreased to -158 MPa for the 250V experiment, -236 MPa for the 350V experiment, and -134 MPa for the 450V experiment. Among all the conditions investigated, the 450V coating maintained the lowest compressive stress values throughout the entire annealing process. This result is consistent with the as-deposited measurements, where the 450V condition already produced the least stressed films due to the lower deposition rate and likely improved structural relaxation during growth.

The 250V experiment showed a stronger stress relaxation between 450°C and 550°C compared to the 350V coating, indicating that the initially denser and more highly stressed film experienced more structural relaxation during thermal treatment. The 350V experiment exhibited the smallest overall stress reduction after annealing and retained relatively high compressive stress values even at elevated temperatures.

Although the 450V experiment produced the lowest average stress values, the room temperature measurements after deposition showed relatively poor stress uniformity across the coating holder. Depending on the substrate position the stress values varied between approximately -320 MPa and -450 MPa. This suggests that higher assisting ion source accelerating voltages may improve average stress reduction while also increasing sensitivity to spatial non-uniformities in ion bombardment conditions across the substrate holder.

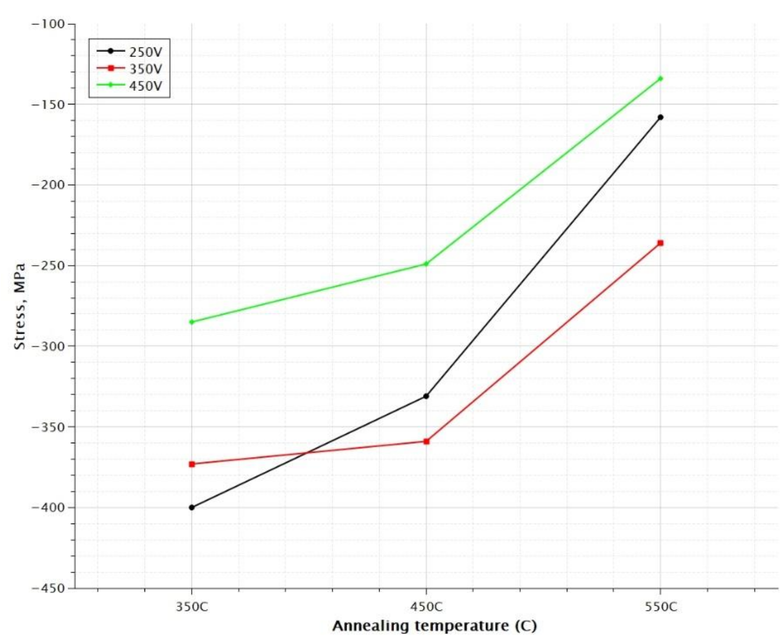

Figure 22. Dependence of coating stress on annealing temperature for samples deposited at different assist ion source accelerating voltages.

The annealing results of the collimating voltage experiments (Figure 23) showed that higher negative voltage values resulted in significantly lower residual stress after thermal treatment. After annealing at 350°C the stress values decreased to -409 MPa for the 900V experiment, -373 MPa for the 1000V experiment, and -359 MPa for the 1100V experiment. The same trend continued at higher annealing temperatures. After annealing at 550°C the 900V coating still retained a compressive stress of approximately -170 MPa, while the 1000V experiment reached -236 MPa. In contrast, the 1100V coating showed a substantially lower residual stress of only around -80 MPa.

The low stress value obtained for the 1100V experiment suggests that the films deposited under higher collimating voltage conditions were more capable of structural relaxation both during deposition and during subsequent thermal annealing. Higher negative voltage likely improved ion beam collimation and produced a more directional and uniform ion bombardment at the substrate surface. Combined with the lower deposition rate observed for the 1100V condition, this may have allowed the growing SiO_2 network to form in a less over-constrained and less defect-rich state [31]. As a result, the film contained lower stored mechanical energy and could relax more efficiently during annealing.

The final stress value of approximately -80 MPa after 550°C annealing is particularly significant because it approaches a near stress-compensated state compared to the strongly compressive as-deposited coatings. Such low residual stress values are highly desirable in precision optical coatings since they greatly reduce substrate bending and wavefront distortion while preserving the optical properties of the deposited films.

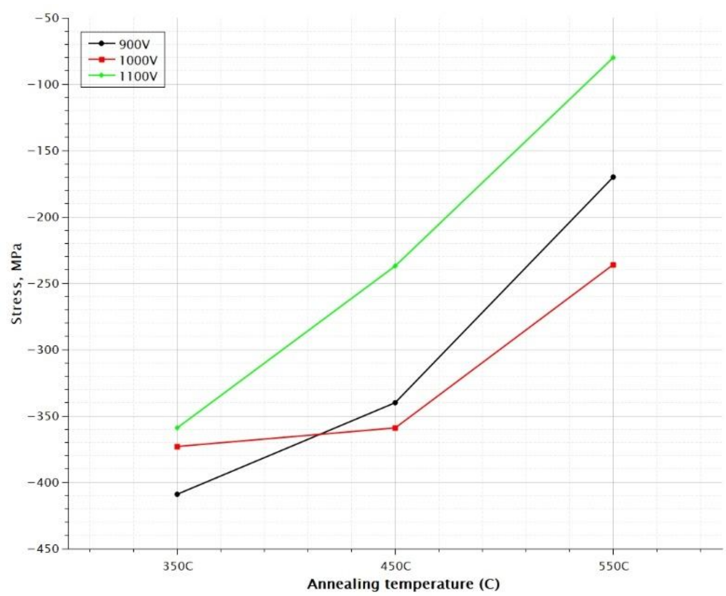

Figure 23. Dependence of residual coating stress on annealing temperature for samples deposited under different assist ion source collimating voltages.

The annealing results of the gas flow experiments showed that all coatings experienced a reduction in compressive stress with increasing annealing temperature (Figure 24). After annealing at 350°C the stress values were approximately -432 MPa for the 75/25 Ar^+/O_2 ratio experiment, -373 MPa for the 50/50 Ar^+/O_2 ratio experiment, and -409 MPa for the 25/75 Ar^+/O_2 ratio condition. At higher annealing temperatures the stress values continued to decrease, with the largest reduction observed for the 75/25 Ar^+/O_2 ratio coating. After annealing at 550°C this sample reached a residual stress of approximately -132 MPa, while the 50/50 Ar^+/O_2 and 25/75 Ar^+/O_2 ratio coatings retained higher compressive stresses of around -236 MPa and -222 MPa respectively.

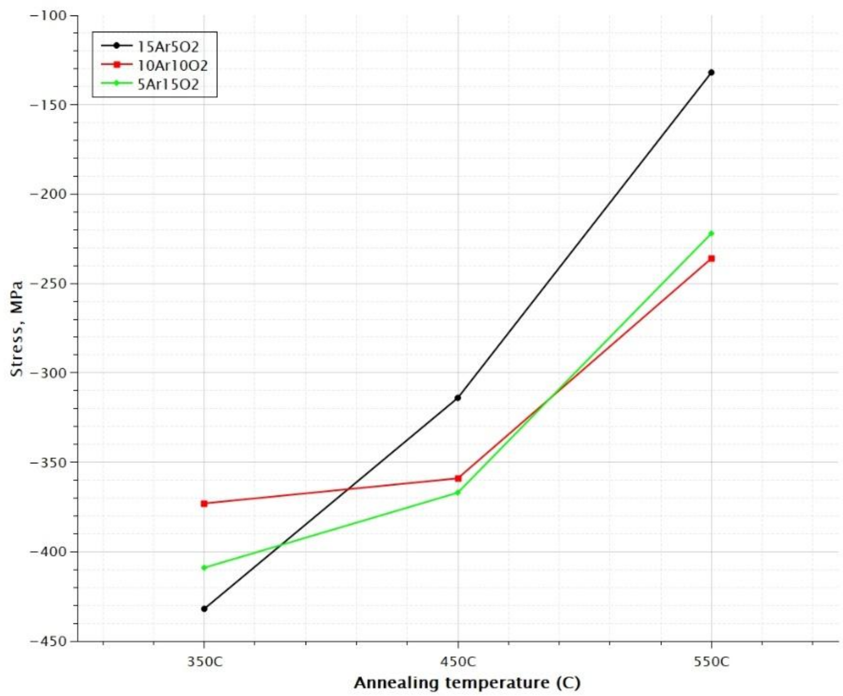

Figure 24. Dependence of residual coating stress on annealing temperature for samples deposited under different assist ion source gas flow conditions.

Although the 75/25 Ar^+/O_2 experiment exhibited the highest compressive stress in the as-deposited state, it also showed the strongest stress relaxation during annealing. This may indicate that the film initially contained a larger amount of stored structural strain which could be more effectively released during thermal treatment. The stronger Ar^+ ion bombardment likely produced a denser and more energetically constrained SiO_2 structure that became more capable of relaxation at elevated temperatures. However, this experiment also showed lower ion beam stability during deposition, which makes the process less favorable from a technological point of view despite the improved stress values after annealing. In comparison, the 50/50 Ar^+/O_2 and 25/75 Ar^+/O_2 ratio conditions resulted in more moderate stress relaxation and retained higher residual stress values after annealing.

Based on the obtained single results, the parameters for the multilayer coating deposition were selected by considering both the residual stress values and the overall process stability. The 1100V collimating voltage was chosen because it demonstrated the best stress relaxation after annealing and resulted in the lowest residual stress values among the investigated collimating voltage conditions. Although the 450V accelerating voltage produced lower average stress values compared to the 350V experiment, the 350V condition showed significantly better stress uniformity across the coating holder and therefore provided more stable deposition conditions. The 50/50 Ar^+/O_2 gas flow ratio was selected because it resulted in the lowest as-deposited stress values and better ion-beam stability during the deposition. As a result, the multilayer coatings were deposited using a 350V accelerating voltage, 1100V collimating voltage, and a reactive gas flow ratio of 10 sccm Ar and 10 sccm O_2 in the assisting ion source.

4.4. Investigation of stress and spectral performance in 1064 nm High-Reflectivity Coatings Deposited under Optimized DIBS Conditions

To evaluate the influence of the assisting ion source on multilayer coating stress and optical performance, a 13-layer high-reflectivity coating for 1064 nm was deposited using alternating Ta_2O_5 and SiO_2 layers with physical thicknesses of 127 nm and 180 nm respectively. The coating deposited with the assisting ion source employed the optimized deposition parameters selected from the monolayer experiments and exhibited an average polarization reflectance of approximately 98% at 1064 nm. To compare the effect of the assisting ion source on the mechanical properties of the multilayer structure, an identical coating with the same layer design and similar average polarization reflectance was also deposited using only the primary ion source without assist source operation. The spectral results can be seen in Figure 25.

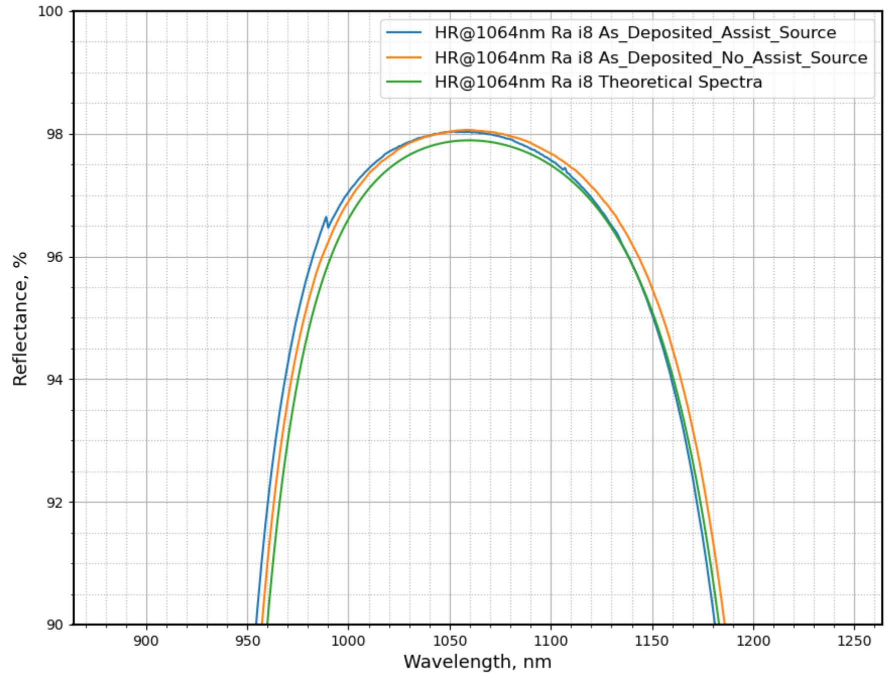

Figure 25. Reflection spectra of HR multilayer coatings deposited with and without assist ion source assistance, together with the theoretical design spectrum.

The measured reflectance spectra of the high-reflectivity coatings deposited with and without the assisting ion source showed very good agreement with the theoretical design spectrum. Both coatings exhibited nearly identical spectral characteristics with an average polarization reflectance of approximately 98% at 1064 nm. No significant spectral shifts or differences in the shape of the reflectance curves were observed between the two deposition approaches, and no negative spectral effects were observed at the target wavelength of 1064 nm. These results indicate that the use of the assisting ion source did not negatively affect the optical performance of the multilayer coating.

The intrinsic stress of the deposited high-reflectivity coatings was evaluated in the as-deposited state across different positions of the coating holder to assess the stress distribution and uniformity of the deposited multilayer structures. The coating deposited with the assisting ion source exhibited average compressive stress values of approximately -320 MPa across the holder, while the coating deposited without the assisting ion source showed higher average compressive stress values of around −370 MPa, this can be seen in Figure 26. The labels C, M, and E correspond to the Centre, Middle, and Edge positions of the substrates with respect to the coating holder geometry.

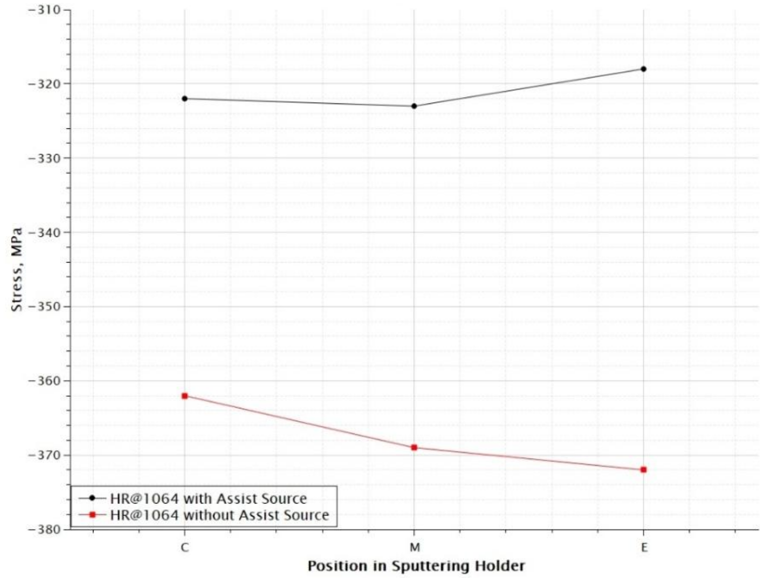

Figure 26. Lateral stress uniformity of HR@1064 coatings deposited with and without assist ion source.

These results confirm the trends observed in the monolayer experiments and demonstrate that the use of the assisting ion source contributes to the reduction of intrinsic stress in multilayer optical coatings. Overall, the DIBS-assisted deposition process reduced the average compressive stress by approximately 50 MPa while maintaining comparable optical performance at the target wavelength of 1064 nm.

The optical measurements of the deposited high-reflectivity coatings showed that both the IBS and DIBS deposited samples exhibited transmission values of approximately 2% at 1064 nm for average polarization, which agrees well with the theoretical coating design.

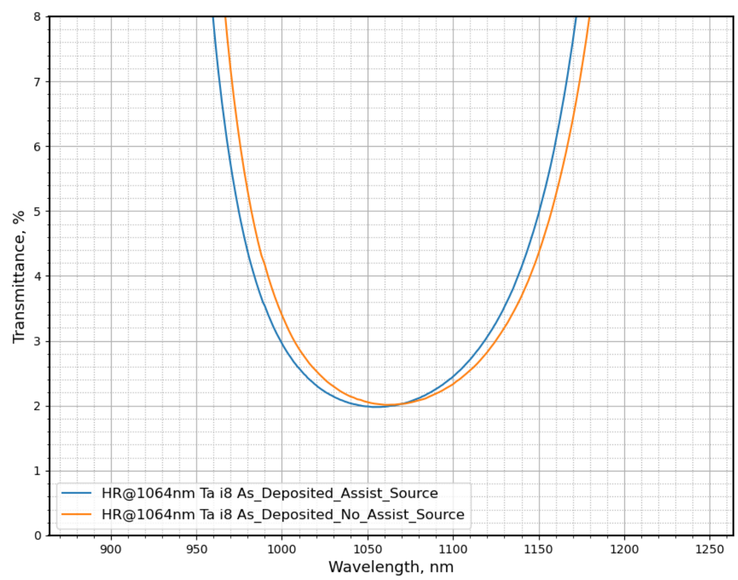

Figure 27. Transmittance spectra of HR multilayer coatings deposited with and without assist ion source assistance, together with the theoretical design spectrum.

Since the measured reflection and transmission values were both close to theoretical values and satisfied the condition $R + T \approx 100\%$, no significant additional absorption introduced by the assisting ion source was observed from the spectral measurements. This indicates that the DIBS process did not negatively affect the optical losses of the coating. Such results are typical for high quality IBS coatings because these films usually exhibit extremely low scattering losses due to their very smooth surface morphology. The roughness of IBS deposited coatings commonly follows the initial substrate surface topography, resulting in very low surface scattering [32].

Although no measurable optical losses were observed from standard spectrophotometric measurements, small absorption losses may still exist at the ppm level. These low absorption values become especially important in high power and high repetition rate laser systems where even very small thermal losses can lead to coating heating and optical damage. In such cases absorption is typically characterized by using highly sensitive methods such as photothermal common-path interferometry (PCI), photothermal deflection spectroscopy, cavity ring-down spectroscopy, or laser calorimetry, which can detect absorption losses in the ppm range [33].

4.5. Residual Stress and Spectral Evolution of Multilayer Coatings after Ex-Situ Annealing

Both previously deposited high-reflectivity multilayer coatings were thermally treated at the same annealing temperatures used for the SiO_2 monolayer experiments. The coatings deposited with and without the assisting ion source were annealed at 350°C, 450°C, and 550°C. After each annealing step the spectral characteristics and residual stress values of the multilayer coatings were measured and compared to evaluate the influence of thermal treatment on the optical performance and stress relaxation of the deposited structures.

Firstly, the reflectance spectra of both multilayer coating experiments deposited with and without the assisting ion source were measured after each annealing step. The measurements showed that the reflectance values remained close to 98% at the target wavelength of 1064 nm for all annealing temperatures. No noticeable decrease in the reflectivity values was observed after thermal treatment, indicating that the annealing process did not negatively affect the overall optical performance of the coatings. The reflectance results of the experiment using the assist source for the multilayer coating can be seen in Figure 28.

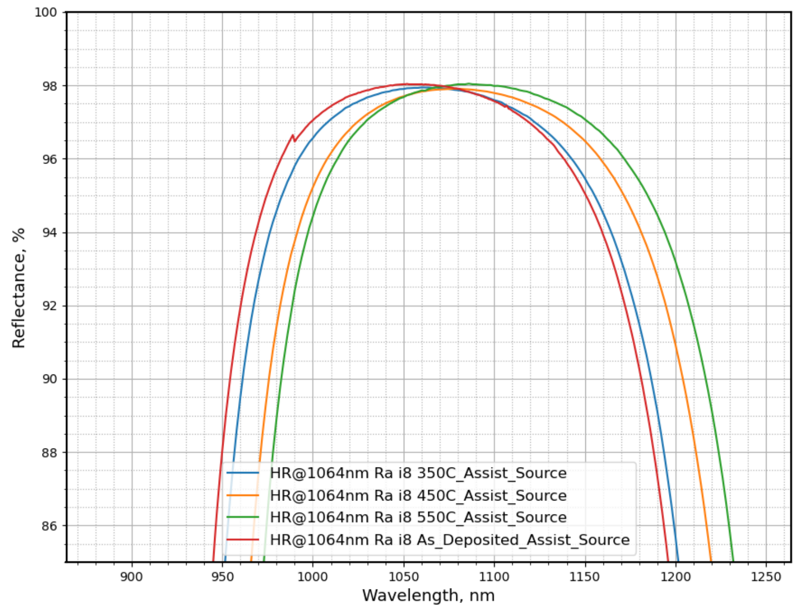

Figure 28. Reflectance spectra of HR@1064 coatings with the assist source in the as-deposited state and after annealing at 350°C, 450°C, and 550°C.

The reflectance results for the experiment without using the assist source can be seen in Figure 29.

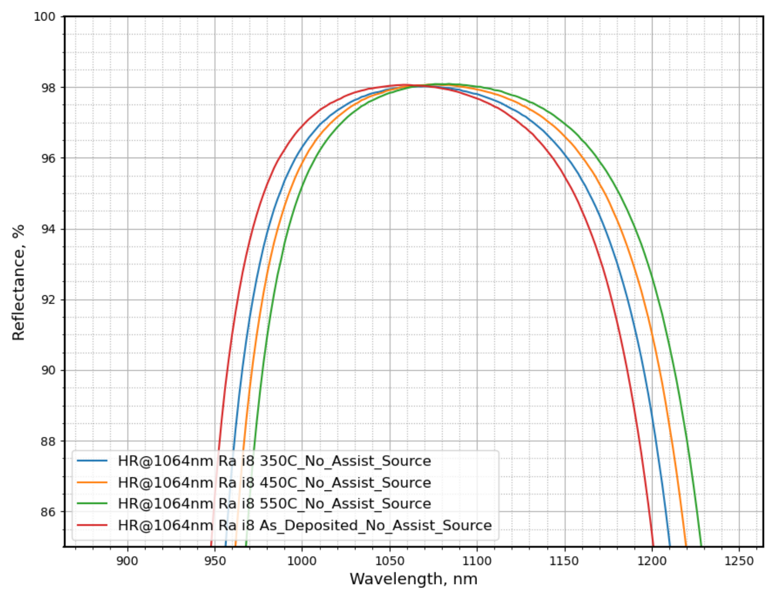

Figure 29. Reflectance spectra of HR@1064 coatings without the assist source in the as-deposited state and after annealing at 350°C, 450°C, and 550°C.

A gradual spectral shift of the high-reflectivity band toward longer wavelengths was observed after annealing, with the magnitude of the shift increasing at higher annealing temperatures. This effect is commonly associated with structural relaxation processes inside the deposited dielectric layers. During annealing the amorphous oxide films partially reorganize into a lower energy state, which can modify the refractive index and optical thickness of the multilayer structure [34]. Since the spectral position of dielectric coatings depends directly on the optical thickness of the layers, even small changes in refractive index or physical thickness can shift the reflectance band toward the infrared region. At higher annealing temperatures the increased atomic mobility enhances these structural changes, resulting in a larger spectral shift. Despite this shift, the overall reflectivity of the coatings remained close to the designed value of approximately 98% at 1064 nm, indicating that the annealing process did not degrade the optical quality of the deposited multilayer structures.

The annealing results showed a strong reduction of compressive stress with increasing annealing temperature for both multilayer coating experiments. In the as-deposited state the coating deposited with the assisting ion source exhibited average compressive stress values of approximately -320 MPa, while the coating deposited without the assisting ion source showed higher stress values of around -370 MPa. After annealing at 350°C the stress values decreased to approximately -215 MPa for the DIBS deposited coating and around -223 MPa for the coating deposited without the assisting ion source. At 450°C the coatings relaxed further to approximately -158 MPa and -125 MPa respectively. The largest stress relaxation occurred after annealing at 550°C, where the DIBS deposited coating reached stress values of approximately −25 MPa, while the coating deposited without the assisting ion source approached a nearly stress-free state and slightly entered the tensile stress region. These stress values can be seen in Figure 30.

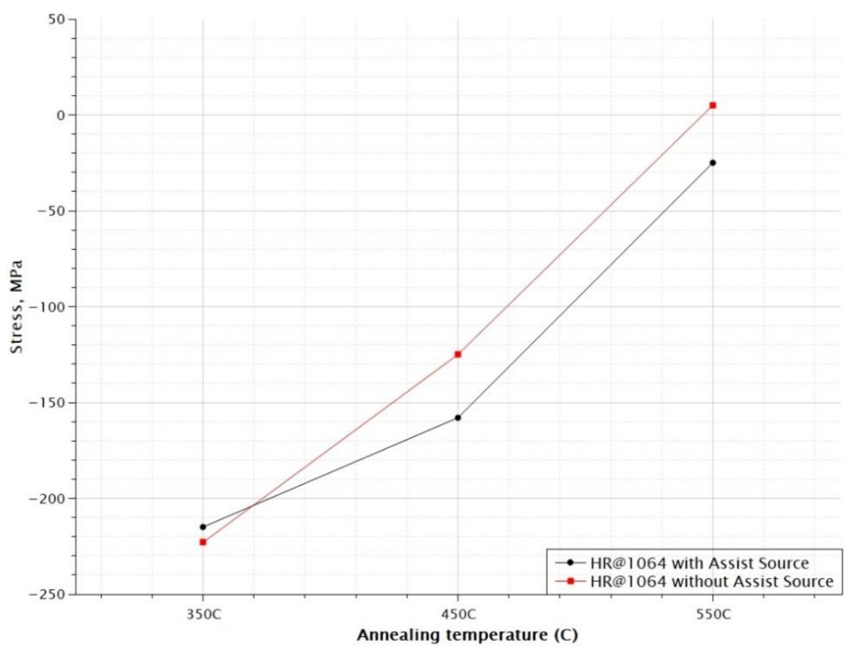

Figure 30. Dependence of residual multilayer coating stress on annealing temperature for samples deposited with and without assist ion source

The stronger relaxation observed for the coating deposited without the assisting ion source is not necessarily a disadvantage, but it may indicate that the multilayer structure was initially in a more energetically unstable state and therefore more prone to structural relaxation during thermal treatment [35]. In contrast, the DIBS deposited coating showed a more gradual relaxation process and maintained slightly compressive stress values even after high temperature annealing, which may suggest that the film structure was already more relaxed during deposition. These results are particularly important because optical coatings cannot always be annealed after deposition. In applications such as thin-disk laser coatings, diffraction gratings, or coatings deposited on temperature-sensitive crystalline substrates, high temperature thermal treatment may not be possible [36]. Therefore, reducing intrinsic stress directly during deposition remains highly important for maintaining substrate flatness and long-term coating stability.

The spectral measurements also showed that multilayer coatings sputtered with and without the help of the assist source and annealed retained expected transmission values close to the expected value of approximately 2% at 1064 nm (see Figure 31-32).

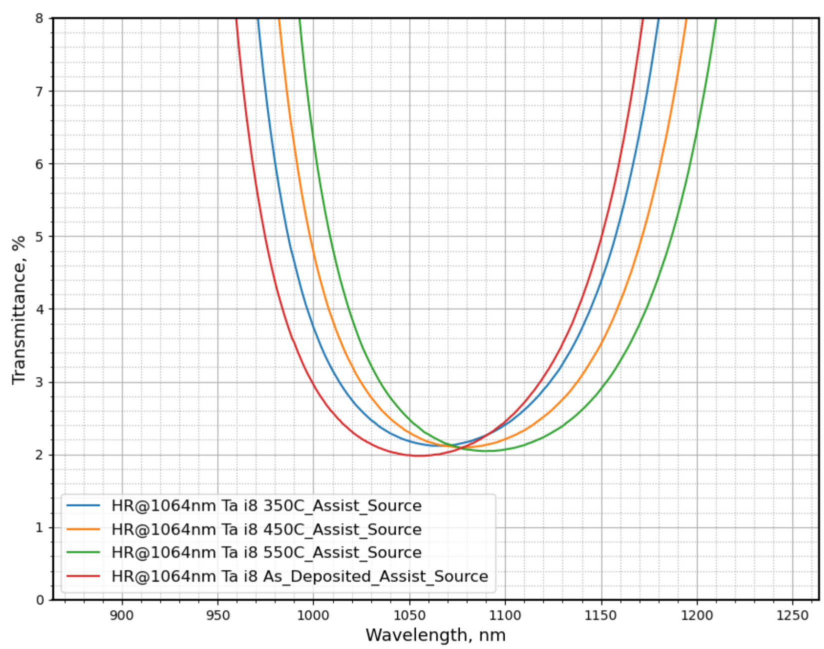

Figure 31. Transmission spectra of HR@1064 coatings with the assist source in the as-deposited state and after annealing at 350°C, 450°C, and 550°C.

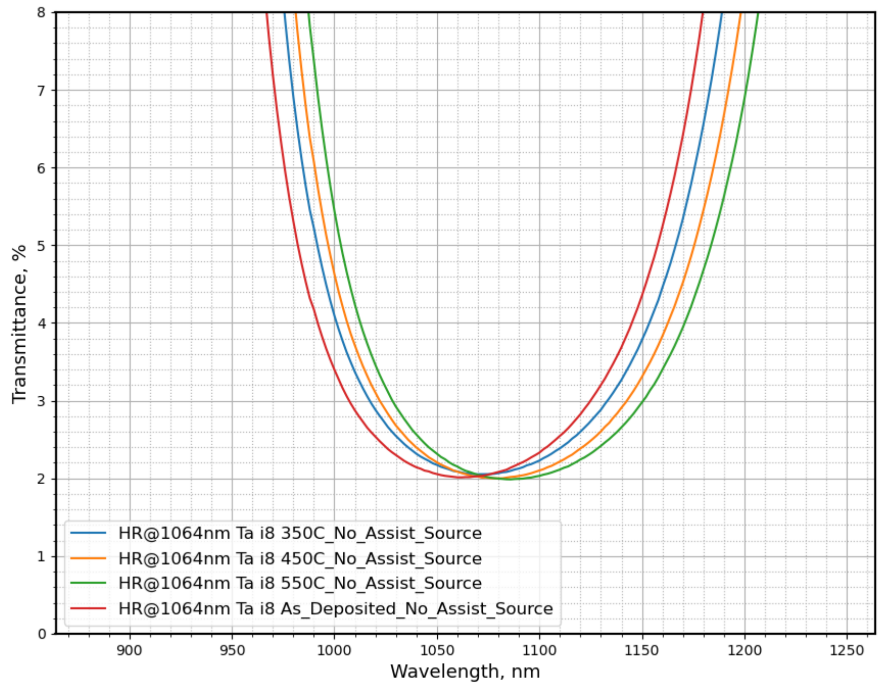

Figure 32. Transmission spectra of HR@1064 coatings without the assist source in the as-deposited state and after annealing at 350°C, 450°C, and 550°C.

Together with the measured reflectance values this indicates that no visible absorption losses were introduced either by the annealing process or using the assisting ion source during deposition. The annealed coatings therefore exhibited optical characteristics like those observed for the as-deposited multilayer coatings. Such results are again typical for high quality IBS coatings, which generally exhibit very low scattering and absorption losses. However small optical losses may still exist at the ppm level inside the multilayer structure and would require more sensitive characterization methods for precise evaluation as discussed before.

5. Main results and conclusions

The performed experiments showed that the assisting ion source parameters have a strong influence on the intrinsic stress of IBS deposited SiO_2 thin films. Increasing the assisting ion source accelerating voltage reduced the compressive stress from approximately -460 MPa at 250V to around -395 MPa at 450V. Similar tendencies were observed when varying the collimating voltage, where the 1100V condition produced the lowest stress values and the strongest stress relaxation after annealing. The reactive gas flow experiments demonstrated that the balanced 50/50 Ar^+/O_2 gas ratio provided the most favourable deposition conditions for minimizing as-deposited stress while maintaining stable deposition conditions.

Ex-situ annealing reduced the compressive stress for all deposited SiO_2 single layers from as high as -450MPa to as low as -80MPa depending on the assist ion source parameters. Higher annealing temperatures promoted structural relaxation inside the films and significantly lowered the residual stress values. The lowest stress after annealing was obtained for the 1100V collimating voltage experiment, where the residual stress decreased to approximately -80 MPa after annealing at 550°C. The results also showed that the initial film structure formed during deposition strongly influenced the subsequent stress relaxation during thermal treatment.

Using the obtained monolayer results, optimized DIBS parameters consisting of a 350V accelerating voltage, 1100V collimating voltage, and a 50/50 Ar^+/O_2 gas flow ratio were selected for the deposition of a 1064 nm high-reflectivity multilayer coating. The multilayer coatings deposited with and without the assisting ion source exhibited very similar spectral characteristics and reflectance values close to the theoretical design of approximately 98% at 1064 nm. At the same time, the multilayer coating deposited with the assisting ion source showed lower average compressive stress values of approximately -320 MPa compared to around -370 MPa for the coating deposited without the assisting ion source.

The annealing experiments performed on the multilayer coatings showed that both structures relaxed significantly with increasing annealing temperature. The coating deposited without the assisting ion source relaxed more strongly and approached a nearly stress-free state after annealing at 550°C, while the DIBS deposited coating maintained slightly compressive stress values. This suggests that the DIBS deposited multilayer structure was already in a more relaxed state directly after deposition. Reflectance and transmission measurements after annealing confirmed that the optical performance of the coatings remained close to the theoretical design and no noticeable additional absorption losses were introduced by either the assisting ion source or the annealing process.

Overall, the obtained results demonstrate that dual ion beam sputtering (DIBS) is an effective method for reducing the intrinsic stress of IBS-deposited SiO_2 films and multilayer optical coatings while preserving high optical quality. The combination of optimized DIBS parameters and ex situ annealing enabled the fabrication of low-stress high-reflectivity coatings suitable for precision optical applications where substrate deformation and flatness control are critical. Furthermore, the lower as-deposited stress achieved using DIBS makes this technique particularly suitable for substrates and coating materials that are sensitive to structural changes during post-deposition annealing.

List of references

[1] Aaron Davenport, Emmett Randel, and Carmen S. Menoni, “Ultra-Low Stress SiO_2 Coatings by Ion Beam Sputtering Deposition,” *Applied Optics* 59, no. 7 (March 1, 2020): 1871, https://doi.org/10.1364/AO.380844.

[2] Massahi, Sonny, Lan M. Vu, Desiree D. Ferreira, et al. 2020. “Balancing of Residual Stress in Thin Film Iridium by Utilizing Chromium as an Underlayer.” In *Space Telescopes and Instrumentation 2020: Ultraviolet to Gamma Ray*, edited by Jan-Willem A. Den Herder, Kazuhiro Nakazawa, and Shouleh Nikzad. SPIE. https://doi.org/10.1117/12.2576298.

[3] Bundesmann, C., I. M. Eichentopf, S. Mändl, and H. Neumann. 2008. “Stress Relaxation and Optical Characterization of TiO2 and SiO2 Films Grown by Dual Ion Beam Deposition.” *Thin Solid Films*, ahead of print. https://doi.org/10.1016/j.tsf.2008.06.032.

[4] Janssen, G. C. A. M. “Stress and Strain in Polycrystalline Thin Films.” *Thin Solid Films* 515, no. 17 (2007): 6654–6664. https://doi.org/10.1016/j.tsf.2007.03.007

[5] Movchan, B A, and Demchishin, A V, "STRUCTURE AND PROPERTIES OF THICK CONDENSATES OF NICKEL, TITANIUM, TUNGSTEN, ALUMINUM OXIDES, AND ZIRCONIUM DIOXIDE IN VACUUM.," *Fiz. Metal. Metalloved. 28: 653-60 (Oct 1969).* (1969)

[6] John A. Thornton, “Influence of Apparatus Geometry and Deposition Conditions on the Structure and Topography of Thick Sputtered Coatings,” *Journal of Vacuum Science and Technology* 11, no. 4 (July 1, 1974): 666–70, https://doi.org/10.1116/1.1312732.

[7] Juliana Jaramillo-Fernandez et al., “Thermal Conductivity of Polycrystalline Aluminum Nitride Films: Effects of the Microstructure, Interfacial Thermal Resistance and Local Oxidation,” in *2015 21st International Workshop on Thermal Investigations of ICs and Systems (THERMINIC)* (2015 21st International Workshop on Thermal Investigations of ICs and Systems (THERMINIC), Paris, France: IEEE, 2015), 1–6, https://doi.org/10.1109/THERMINIC.2015.7389602.

[8] Anders, Andre. “A Structure Zone Diagram Including Plasma-Based Deposition and Ion Etching.” *Thin Solid Films* 518, no. 15 (2009): 4087–4090. https://doi.org/10.1016/j.tsf.2009.10.145.

[9] “Impact of Wafer Bow in TSVs,” accessed June 4, 2025, https://www.iue.tuwien.ac.at/phd/singulani/dissse17.html.

[10] Stoney, G. G., and C. A. Parsons. “The Tension of Metallic Films Deposited by Electrolysis.” *Proceedings of the Royal Society of London. Series A, Containing Papers of a Mathematical and Physical Character* 82 (1909): 172–175. https://doi.org/10.1098/rspa.1909.0021.

[11] C.A. Davis, "A Simple Model for the Formation of Compressive Stress in Thin Films by Ion Bombardment," *Thin Solid Films* 226, no. 1 (April 15, 1993): 30–34, https://doi.org/10.1016/0040-6090(93)90201-Y.

[12] Valentini, A., D. Quaranta, M. G. Valentini, and G. Barucca. "Dual-Ion-Beam Sputter Deposition of TiN Films." *Journal of Applied Physics* 69, no. 10 (1991): 7360–7367. https://doi.org/10.1063/1.347596

[13] E. Randel et al., "Ultra-Low Stress SiO2 Ion Beam Deposition Coatings," in *Optical Interference Coatings Conference (OIC) 2019* (Optical Interference Coatings, Santa Ana Pueblo, New Mexico: OSA, 2019), WC.5, https://doi.org/10.1364/OIC.2019.WC.5.

[14] Thomas Begou and Julien Lumeau, "Accurate Analysis of Mechanical Stress in Dielectric Multilayers," *Optics Letters* 42, no. 16 (August 15, 2017): 3217, https://doi.org/10.1364/OL.42.003217.

[15] Jinlin Bai et al., "Ultra-Low Stress High Reflective Film by Dual-Ion-Beam Sputtering Deposition," *Optical Engineering* 61, no. 03 (November 25, 2021), https://doi.org/10.1117/1.OE.61.3.031203.

[16] McNeil, J. R., R. T. Hodgson, R. E. Martin, and J. E. McGahan. "Ion-Assisted Deposition of Optical Thin Films: Low Energy vs High Energy Bombardment." *Applied Optics* 23, no. 4 (1984): 552–559. https://doi.org/10.1364/AO.23.000552.

[17] Kim, Namjun, and Jonathan F. Stebbins. 2013. "Effects of Annealing on the Structure of Ion Beam Sputtered Amorphous Tantalum Oxide: Oxygen-17 NMR Spectra and Relaxation Times." *Journal of Non-Crystalline Solids*, ahead of print. https://doi.org/10.1016/j.jnoncrysol.2013.07.003.

[18] Kičas, Simonas, Ugnius Gimževskis, and Simas Melnikas. 2016. "Post Deposition Annealing of IBS Mixture Coatings for Compensation of Film Induced Stress." *Optical Materials Express* 6 (7): 2236. https://doi.org/10.1364/OME.6.002236.

[19] Begou, Thomas, and Fabien Lemarchand. "High-Performance Thin-Film Optical Filters with Stress Compensation." *Journal of the Optical Society of America A* 36, no. 11 (2019): C113–C119. https://doi.org/10.1364/JOSAA.36.00C113

[20] Amotchkina, Tatiana, Michael K. Trubetskov, Yurij Pervak, Laszlo Veisz, and Vladimir Pervak. 2014. "Stress Compensation with Antireflection Coatings for Ultrafast Laser Applications: From Theory to Practice." *Optics Express* 22 (24): 30387. https://doi.org/10.1364/OE.22.030387.

[21] Mohammad Yeakub Ali, Wayne Hung, and Fu Yongqi, "A Review of Focused Ion Beam Sputtering," *International Journal of Precision Engineering and Manufacturing* 11, no. 1 (February 2010): 157–70, https://doi.org/10.1007/s12541-010-0019-y.

[22] Gerhard Bauer, “Absolutwerte Der Optischen Absorptionskonstanten von Alkalihalogenidkristallen Im Gebiet Ihrer Ultravioletten Eigenfrequenzen,” *Annalen Der Physik* 411, no. 4 (1934): 434–64, https://doi.org/10.1002/(ISSN)1521-388910.1002/andp.v411:410.1002/andp.19344110405.

[23] Elma Schmidbauer GmbH. n.d. “Systems.” Accessed May 15, 2026. https://www.elma-ultrasonic.com/en/systems.

[24] Jena, S., R. B. Tokas, S. Thakur, and N. K. Sahoo. 2015. *Characterization of Optical Thin Films by Spectrophotometry and Atomic Force Microscopy*. 6 (1).

[25] “PHOTON RT UV-VIS-MWIR Spectrophotometers for Coaters.” n.d. Accessed May 15, 2026. https://www.essentoptics.com/eng/products/spectrophotometers/photon_rt/.

[26] www.lighttrans.com. n.d. “Fizeau Interferometer for Optical Testing.” Accessed May 16, 2026. https://www.lighttrans.com/use-cases/application/fizeau-interferometer-for-optical-testing.html.

[27] Scia Systems GmbH. n.d. “Scia Opto 300.” Accessed May 16, 2026. https://www.scia-systems.com/products/ion-beam-sputtering/scia-opto-300.

[28] Oxford Instruments Plasma Technology, “An Introduction to Ion Beam Etching,” AZoM, October 15, 2012, https://www.azom.com/article.aspx?ArticleID=7533.

[29] Peter Sigmund, “Theory of Sputtering. I. Sputtering Yield of Amorphous and Polycrystalline Targets,” *Physical Review* 184, no. 2 (August 1969): 383–416, https://doi.org/10.1103/PhysRev.184.383.

[30] Morgan, R., C. J. Sutcliffe, and W. O’Neill. “Experimental Investigation of Nanosecond Pulsed Nd:YAG Laser Re-Melted Pre-Placed Powder Beds.” *Rapid Prototyping Journal* 7, no. 3 (2001): 159–172. https://doi.org/10.1108/13552540110395565

[31] D J Smith et al., “Reducing the Stress of Hafnia/Silica Multilayers with Ion Assisted Deposition for Use in High-Power Diffraction Gratings,” *Th Annual Technical Conference Proceedings.*, n.d.

[32] Kraus, J., J. Davis, B. Rubin, O. Lyngnes, and A. Ode. 2014. “Improving Throughput of Ion Beam Sputtered Optical Films.” 245–48. https://doi.org/10.14332/svc13.proc.1086.

[33] Welsch, E., and D. Ristau. “Photothermal Measurements on Optical Thin Films.” *Applied Optics* 34, no. 31 (1995): 7239–7253. https://doi.org/10.1364/AO.34.007239

[34] Colace, Stefano, Shima Samandari, Massimo Granata, et al. 2024. “Monitoring the Evolution of Optical Coatings during Thermal Annealing with Real-Time, in Situ Spectroscopic Ellipsometry.” *Classical and Quantum Gravity* 41 (17): 175016. https://doi.org/10.1088/1361-6382/ad672c.

[35] L. Skuja et al., “Oxygen-Excess-Related Point Defects in Glassy/Amorphous SiO2 and Related Materials,” Nuclear Instruments and Methods in Physics Research Section B: Beam Interactions

with Materials and Atoms 286 (September 2012): 159–68, https://doi.org/10.1016/j.nimb.2012.02.038.

[36] Chen, Jinju, and S. J. Bull. 2011. "Approaches to Investigate Delamination and Interfacial Toughness in Coated Systems: An Overview." *Journal of Physics D: Applied Physics* 44 (3): 034001. https://doi.org/10.1088/0022-3727/44/3/034001.